ORTA DOĞU TEKNİK ÜNİVERSİTESİ
MIDDLE EAST TECHNICAL UNIVERSITY
KUZEY KIBRIS KAMPUSU ♦ NORTHERN CYPRUS CAMPUS

ASE 435 – PROPULSION SYSTEMS II

Ramjet Engine Project

Development of a Ramjet Engine Design Code and CFD Analysis of Engine Intake for the Design Point Mach Number

05.02.2022

Group Members:

Faruk Çorum 2021111
Berkay Cihan 2318020
Ömer Hakan Bozkurtoğlu 2156206
Ravian w. Simiyu 2337905

Instructor Name: Dr. Sıtkı Uslu

Course Assistant: Özlem Mert / Joseph G. Waweru

Group Name: FireFly Jetx

TABLE OF CONTENTS

ABSTRACT iii
NOMENCLATURE iv
1. INTRODUCTION 1
2. HISTORICAL TIMELINE 2
3. RAMJET APPLICATIONS 3
3.1. Missile Applications 3
3.2. Aircraft Applications 3
4. COMPONENTS ANALYSIS 5
4.1. Inlet Models 6
4.1.1. Internal Compression 6
4.1.2. External Compression 7
4.1.3. Mixed Compression 7
4.1.4. Inlet Design and Sizing 8
4.1.5. Inlet Performance Parameters 8
4.2. Combustion Chamber 9
4.2.1. Jet Engine Fuels 9
4.2.2. Types of Fuel Injectors 11
4.2.2.1. Parallel Fuel Injection 11
4.2.2.2. Normal Fuel Injection 12
4.2.2.3. Transverse Fuel Injection 12
4.2.2.3.1. Strut Injectors 12
4.2.2.3.2. Baronage Injection System 13
4.2.2.3.3. Pulsed Injector 13
4.2.3. Positioning of Injectors 14
4.2.3.1. Flameholders 14
4.2.4. Useful Equations in the Combustion Chamber 15
4.3. Nozzle 16
4.3.1. Flow Through a Convergent-Divergent (C-D) Nozzle 17
4.3.2. Nozzle Geometric Configurations 18
4.3.2.1. Conical nozzle 18
4.3.2.2. Belli Nozzle 18
4.3.2.3. Single expansion ramp nozzle 18
4.3.2.4. Dual Bell and Contoured Nozzle 18

4.3.3. Ramjet Engine Analysis for the Nozzle Section 19
5. RESULTS AND DISCUSSION 20
5.1. Engine Design 20
5.2. Analysis of Important Parameters 24
5.3. The Analysis of Engine Performance and Comparison 26
6. COMPUTATIONAL FLUID DYNAMICS (CFD) RESULTS 27
6.1. Inlet Design 27
6.2. Nozzle Design 28
7. CONCLUSION 30
REFERENCES 31
APPENDICES 34
A) MATLAB Codes 34
A.1. Ramjet Engine 34
A.2. Engine Inlet 38
B) CAD Design 40
B.1. CAD Drawing for the ConDi Nozzle 40

ABSTRACT

In the project, the ramjet is analyzed and evaluated in detail so as to create a unidimensional (1D) MATLAB code for the ramjet engine design. The project contains a thorough Computational Fluid Dynamics (CFD) of the inlet and nozzle parts of the ramjets. The CFD analysis was done on Ansys software. The ramjet engine design is also evaluated by the Gasturb 14 software in order to check the performance characteristics of the engine. Graphs are also obtained from the MATLAB code and checked whether they agree with our theory and concepts. Important variables that were considered in our design are the number of ramps chosen. Furthermore, the type of compression is discussed and used in our engines. Finally, the combustor is evaluated, taking into account the types of fuels and fuel technologies available. The nozzle concepts are included as well.

NOMENCLATURE

A:	*Area* $[m^2]$
A^*:	*Choked area* $[m^2]$
a:	*Local speed of sound* $[m/s]$
A_{ref}:	*The reference area* $[m^2]$
c_p:	*Pressure coefficient*
D_{add}:	*Additive drag* $[N]$
D_r:	*Ram drag* $[N]$
F_g:	*Gross thrust* $[N]$
F_n:	*Net thrust* $[N]$
H:	*Height* $[m]$
h:	*Specific enthalpy* $[J/kg]$
h_t:	*Specific total enthalpy* $[J/kg]$
L:	*Lift* $[N]$
M:	*Mach number*
$\dot{m}$:	*Mass flow rate* $[kg/s]$
$\dot{m}_f$:	*Fuel mass flow rate* $[kg/s]$
$\dot{m}_0$:	*Air mass flow rate* $[kg/s]$
$\dot{m}_p$:	*Propellant mass flow rate* $[kg/s]$
p:	*Static pressure* $[bar, Pa]$
p_t:	*Total pressure* $[bar, Pa]$
Q_R:	*Fuel heating value* $[kJ/kg]$
q:	*Dynamic pressure* $[bar, Pa]$
T:	*Temperature* $[K]$
T_t:	*Total temperature* $[K]$
t:	*Time* $[s]$
u:	*Gas speed* $[m/s]$
V:	*Volume* $[m^3]$
V:	*Speed* $[m/s]$
V_m:	*Mean speed* $[m/s]$
V':	*Relative speed* $[m/s]$
W:	*Weight* $[N]$
W_a:	*The actual work* [J]
W_{real}:	*The real compressor work* [J]
W_s:	*Isentropic compressor work* [J]
w:	*Specific work* $[J/kg]$
γ:	*Ratio of specific heats*
φ:	*Cooling effectiveness parameter*
ρ:	*Fluid density* $\left[\frac{kg}{m^3}\right]$
μ:	*Coefficient of viscosity* $\left[\frac{N*s}{m^2}\right]$
η_o:	*Overall efficiency*
$\eta_{T_{HP}}$:	*Turbine efficiency for the HP*
$\eta_{T_{LP}}$:	*Turbine efficiency for the LP*

Abbreviations and acronyms

AB:	*AfterBurner*
AFR:	*Air Fuel Ratio*
BPR:	*ByPass Ratio*
$ConDi$:	*Convergent-Divergent Nozzle*
FPR:	*Fan Pressure Ratio*
HPC:	*High Pressure Compressor*
HPT:	*High Pressure Turbine*
LPC:	*Low Pressure Compressor*
LPT:	*Low Pressure Turbine*
$Max\ Dry$:	*W/o AB*
OPR:	*Overall Pressure Ratio*
SLS:	*Standard Sea-Level*
T/W:	*Thrust to Weight Ratio*
TET:	*Turbine Entry Temperature*

Subscripts

a:	*Actual*
f:	*Fuel*
g:	*Gross*
m:	*Mean*
max:	*Maximum*
n:	*Net*
p:	*Propellant*
r:	*Relative*
rev:	*Reversible*
s:	*Isentropic*
t:	*Total*

Superscripts

$*$:	*Critical or sonic state*

1. INTRODUCTION

A ramjet engine provides a simple, lightweight propulsion system for high-speed flight. Similarly, the supersonic combustion ramjet provides high thrust and low weight for hypersonic flight speeds. Ramjets, unlike turbojet engines, have no moving parts and only have a combustion chamber containing the inlet, fuel injector, and flame holder. Due to the aircraft's forward motion, significant volumes of ambient air are strongly attracted into the engine inlet when placed on a high-speed aircraft. The air slows as it travels through the inlet, converting the velocity-dependent dynamic pressure to higher static pressure. The air pressure at the inlet's exit is substantially higher than the free flow. The flow out of a ramjet's inlet is always subsonic, regardless of whether the free flow rate is subsonic or supersonic. At the same vehicle speed, the flow out of a scramjet intake is supersonic and has less shock loss than a ramjet inlet [1].

In comparison to most other jet engines, the design of the ramjet engine is straightforward. Compressed air, which is pumped into the engine as it reaches high speeds, is the source of engine power. As a result, it only operates after the plane or device reaches specified speeds, not before. At sea level, the ramjet reaches maximal efficiency around Mach 3, or 2,283 mph (3,675 km/h), which is three times the speed of sound. Ramjets can travel at speeds ranging from 0.5 to 6 times the speed of sound. Before Mach 1, the low pressure creates relatively little push. When the Ramjet reaches more than Mach 5, it loses efficiency [2].

- ## Description of Ramjet Problem

To compress the incoming air, a ramjet uses the forward motion of the engine instead of the compressor. This is because ramjets cannot generate thrust at zero airspeeds, and therefore they cannot propel aircraft forward from a standstill. As a result, ramjet-powered airplanes need assistance to take off until thrust is built up. A ramjet should run at supersonic speeds of roughly Mach 3 to get the most efficient performance. Ramjet can run at speeds up to 6 Mach. The main aim of the project is to develop a one-Dimensional design code that estimates the performance of a ramjet engine at various flight speeds ranging from 2 to 6 using analytical and/or empirical, semi-empirical correlations. One of the most important components of this project is the number of ramps used in the intake design. As the flight speed increases, the number of ramps also increases. Also, whether external, internal, or hybrid compression is used for the design, it is critical to understand the state of input compression [31].

2. HISTORICAL TIMELINE

Scientists began work on ramjet propulsion in the early 1900s. The ramjet engine is extremely simple. It contains no real moving components and no turbines, compressors, stators, or other parts that block the flow of the engine, making it extremely fuel-efficient and eliminating the need for an oxygen source. A rocket would significantly reduce the weight and risks of owning one of the most flammable cargoes on the planet.

In 1913, ramjet was a device invented and patented by René Lorin in France. Prototype construction led to frustration due to the use of unsuitable materials. Albert Fonó, a Hungarian inventor, discovered a means to extend the range of his guns in 1915. The low-range cannon's high-range capability is enabled by adding a ramjet unit to the launch mechanism, allowing a high-weight gun to be fired from a low-weight gun launcher. Fonó tried to sell his innovation to the Austro-Hungarian army, but they turned it down. Hellmuth Walter created a gas-powered test engine in 1936. Afterward, theoretical work was continued by BMW and Junkers. Eugen Sänger developed a ramjet engine with a high-temperature combustion chamber in 1941. Then, when oil shortages occurred in Germany during the war, tests with compressed coal dust blocks continued, but they were ineffective due to low combustion [3].

In the late 1930s, the Soviet Union developed the first ramjet engines, and the world's first ramjet-powered aircraft flight took place in December 1940. The maiden flight of the Leduc 010, propelled solely by a ramjet engine, took place in 1949, demonstrating its exceptional capabilities. Before the air could be compressed sufficiently for the engine to start igniting, the jet had to achieve Mach 0.5. The jet was first attached to a rocket to accelerate, but it was then placed atop a Languedoc 31 to bring it to the proper altitude where it would separate and drop until it reached critical speed at which the engine could operate. The ramjet proved to be a landmark in avionics for flights up to Mach 5, but a major flaw was discovered at higher speeds. In a ramjet, combustion must take place at subsonic speeds. Due to the powerful shock waves created at the aircraft intake, the air slows down to subsonic speeds for a vehicle that exceeds the speed of sound. The shock waves create such large performance losses above Mach 5 that the engine is unable to generate thrust, forcing the jet to slow down. In the 1960s, an improved ramjet was created with a supersonically operating burner. The engine's improved ramjet reduces shock wave flow loss, allowing it to provide adequate thrust for hypersonic travel or speeds of Mach 15. The scramjet is substantially more efficient than a rocket that must carry all of its oxygen on board since it uses external air to power the combustion chamber. Scramjets, which are designed for hypersonic flight, will not work at speeds less than Mach 3 and will require the use of a rocket to reach essential engine stall speeds [4].

3. RAMJET APPLICATIONS

Ramjet engines are used for the propulsion of both missiles and aircraft. Various examples of applications in both areas are given in the following sections.

3.1. Missile Applications

Most missile variants use ramjet engines, which are described in the following subsections [5].

- Air-to-air missiles

Medium-range missiles with ramjet engines can maintain a greater average velocity and increase their range over their attack area. MBDA Meteor is an example (scheduled to enter service in 2015).

- Air-to-surface missiles

Examples are EADS/AMM, ASMP, ASMP-A, Radouga Kh41 Moskit and Zvezda Kh31P

- Surface-to-air missiles

Examples are MBDA and LFK NG (USA), Bloodhound Mk2, Rapier and Sea Dart (UK), Mistral and Eurosam Aster (France), and Aspide (Alenia consortium)

- Anti-ship missiles

Examples are Machinostroenie 3 K55, Yakhont (SS N26), ANS (liquid-fueled ramjet; reaches Mach 4 Range 25 km), and C101 & C103 (ranges 50 and 100 km).

3.2. Aircraft Applications

To overcome the difficulties of the pure ramjet engine, one variant of the pure ramjet engine was joined to another type of engine (piston/turbojet/turbofan). Following is a list of ramjet engines organized by country [5].

- France

Two different ramjets were produced, namely:

a. The Leduc 0.10 had been a study aircraft with a Leduc ramjet engine specifically designed to remove it from the aircraft transporting it to altitude. It attained Mach 0.84 at 26,000 feet. It flew in October 1947, generating 15.7 kN of force [5].

Figure 1. Leduc 0.10.[6]

b. In the mid-1950s, Nord Aviation designed and produced the Nord 1500 Griffon, a pioneering ramjet-powered Mach 2 fighter plane.

- Germany

Hellmuth Walter created a natural gas-powered test engine in 1936. DFL's Eugen Sanger presented a ramjet engine with a high combustion chamber temperature in 1941. Additionally, he created ramjet pipes with huge diameters and conducted combustion experiments at speeds of up to 200 m/s [5].

- Japan

The ATREX engine is an example of the AirTurbo Ramjet (ATR), a "combined cycle" engine designed to overcome the limits of pure ramjet engines. It functions as a traditional turbojet at subsonic speeds, and below Mach 6, it operates as a fan-assisted ramjet [5].

- United States of America

a. The Lockheed X-7 was an aircraft ramjet test site. A B-29 or B-50 Superfortress aircraft carrier carried it into the air. After launch, the booster rocket ignited, accelerating the vehicle to 1000 mph (1625 km/h).
b. A hybrid engine, part turbojet and part ramjet powers the SR-71 high-speed reconnaissance aircraft (defined as the turbo-ram engine).

4. COMPONENTS ANALYSIS

A complete Ramjet Engine consists of three main components.

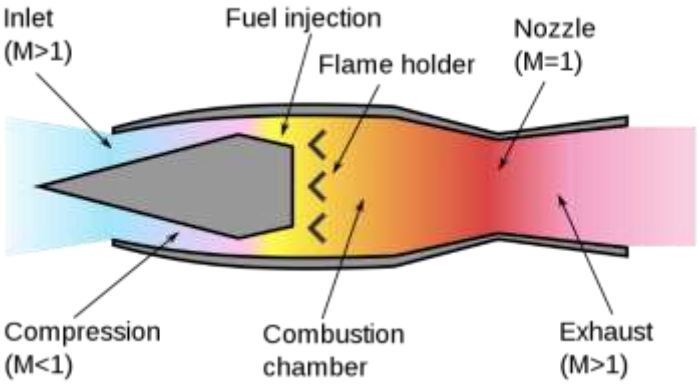

Figure 2. Ramjet components.[7]

The figure 2 shows the components along with their functions. These five modules are Intake (Diffuser), Combustion (Fuel injectors, Flame Holder), and Exhaust nozzle.

The first component of any air-breathing engine is the intake. The entrance can have a circular/oval or rectangular entrance. Also, it can have fixed or variable field input. For shocks captured during supersonic flight speeds, supersonic ramjets may have intake cones (also known as shock cones, intake center bodies, or spikes) or compression ramps. External/internal (mixed) compression reception is selected in such cases. These oblique shocks must be followed by a strong normal shock to reduce the airflow to subsonic velocities before entering the combustion chamber [8].

Combustion chambers are designed afterburner, in which chemical processes create energy. A ramjet burner may safely run at stoichiometric fuel/air ratios since there is no downstream turbine, resulting in a combustion chamber exit stagnation temperature on the order of 2400 K for kerosene. Inside the combustion chamber, fuel is introduced, mixed with some air, and then ignited by one or more igniters. The residual air is utilized to keep things cool. The combustion process occurs at near-constant pressure. Due to friction and the fuel-air combination, there will be a minor reduction in overall pressure in the burner. The fuel combustion will be replicated as heat, removing the complexities of the chemical process [8].

The nozzle is the last and most critical component in all jet engines. It converts the kinetic energy of the hot gas jet, which creates thrust from pressure and thermal energy. The geometry of the nozzles can be fixed or changeable. There may also be segments that are convergent or convergent-divergent. Finally, the nozzles may be clogged or open. The nozzle flow is modeled as polytrophic expansion with a given isentropic efficiency. A typical nozzle efficiency rating is 99 percent [8].

4.1. Inlet Models

The ramjet's most important feature is likely its intake design. Jet engines use the compressor to increase air pressure, but pulse-jet engines use the pressure waves from earlier cycles to compress a new fuel-air charge. However, because this is all that is available, a ramjet can only rely on the compression produced by air passage into the intake. This pressure recovery is limited at subsonic speeds, but huge ram-pressure ratios become attainable as the Mach number rises. Also, a ramjet has the advantage of being able to be built to only function at supersonic speeds, eliminating the need for bypass ducts, rounding of the intake lip edges, and other features common in aircraft with these intakes [9].

Internal compression, external compression, and mixed compression are the three primary types of inlet models, which are distinguished by the supersonic compression wave system [9].

4.1.1. Internal Compression

The compression achieved by this intake design is accomplished by generating a sequence of internal oblique shock waves, with a terminal or 'normal' shock wave located near the throat. In order to place the shock waves and avoid air overflowing around the engine, this intake requires changeable geometry [11].

At first appearance, this intake appears to support the theory that an intake might be designed similarly to a converging-diverging nozzle in reverse, with compression created without the need of shock waves, resulting in lower losses. Due to the fixed intake geometry, shock waves will undoubtedly arise at the throat during off-design circumstances, causing the mass flow rate down the throat to be reduced. As a result, air piles up in the intake, causing a shock to occur across the intake lip and air to spill over the entrance in the subsonic flow aft of the shock wave [11].

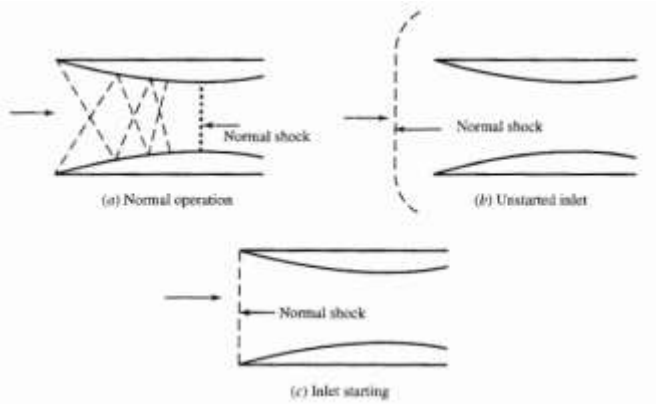

Figure 3. Internal compression inlet.[11]

Compression is achieved by a sequence of internal oblique shock waves followed by a terminal normal shock downstream of the throat, as shown in Figure 3-(a).

To swallow the usual shock, this form of intake needs a changeable throat area (during starting). Fast reaction bypass doors are also required downstream of the throat to allow the typical shock to be positioned appropriately under variable flight and engine conditions [11].

4.1.2. External Compression

This intake is based on oblique shock waves generated by a projection forward of the inlet colliding with the intake lip and producing a normal shock wave. A ‘pitot’ intake is an airflow compression system that relies purely on natural shock. Since it is simple to construct, manufacture, and has a short length, this is the most basic sort of supersonic intake [11].

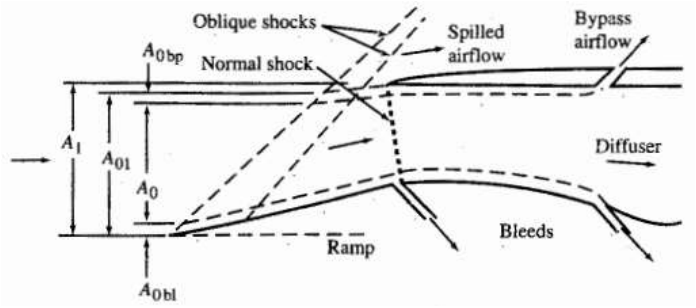

Figure 4. External compression inlet and flow areas.[9]

The figure 4 illustrates the external compression intake, which is compressed by one or more oblique shocks followed by a normal shock or a single normal shock.

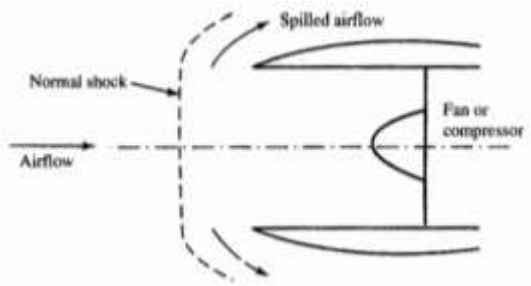

Figure 5. Pitot or normal shock inlet.[9]

A pitot inlet, also known as a normal shock inlet, is an external compression inlet that produces compression with only a single normal shock, as depicted in Figure 5. The pitot inlet is straightforward, short, light, and cheap [9].

4.1.3. Mixed Compression

The mixed compression inlet is utilized at Mach numbers greater than 2.5 to achieve a suitable total pressure ratio (using the requisite number of oblique shocks) while minimizing cowl drag. The external compression intake is simpler, heavier, and more expensive than the mixed compression inlet [10].

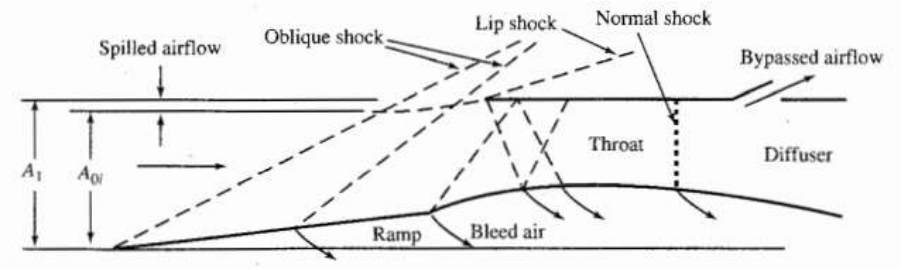

Figure 6. Two-dimensional mixed compression inlet.[9]

Compression is achieved at the usual mixed compression inlet, as shown in Figure 6, by external oblique shocks, internal reflected oblique shocks, and the terminal normal shock.

The normal shock should be located just downstream of the input throat to reduce overall pressure loss while retaining a stable working location. The mixed compression inlet, like the internal compression inlet, necessitates both fast-acting bypass doors and a variable throat area. However, due to the external oblique shock system in the mixed compression inlet, the variance in the inlet throat area is significantly less than that of the internal compression inlet [9].

4.1.4. Inlet Design and Sizing

Because of the variations like supersonic and subsonic flows, designing and sizing a supersonic intake is significantly more complicated than designing and sizing a subsonic inlet. The supersonic inlet supports both subsonic and supersonic flight Mach numbers. The inlet's capture and throat portions must be large enough to allow the engine, boundary-layer bleed system, and other airflow requirements. The capture area A1 of the inlet is sized to catch the appropriate airflow for supersonic flying conditions. Variable geometry inlet design is sometimes required to satisfy the total pressure recovery target of military specification MIL-E-5008B and keep installation losses low because this airflow varies with flight Mach number and engine throttle setting [9].

4.1.5. Inlet Performance Parameters

Total pressure recovery and flow distortion are the two most critical performance criteria of supersonic inlets. Since it directly impacts the engine thrust force, the inlet's total pressure recovery (TPR) is another important factor determining inlet performance. Total pressure recovery is calculated by dividing the total pressure of the engine face P_{in} by the total pressure of the free stream (P_o) flow, as illustrated below [12]:

$$TPR = \frac{P_{in}}{P_o} \tag{1}$$

Flow separation occurs when inlets are subjected to an adverse pressure gradient. Total pressure loss and a lack of consistency in total pressure distribution in each section are caused by flow separation. Flow Distortion (FD) is the name for this phenomenon, and it is quantified in Equation (9) as follows [12]:

$$FD = \left(\frac{P_{in}}{P_{o\,max}}\right) - \frac{\left(\frac{P_{in}}{P_{o\,min}}\right)}{\left(\frac{P_{in}}{P_{o\,avg}}\right)} \tag{2}$$

4.2. Combustion Chamber

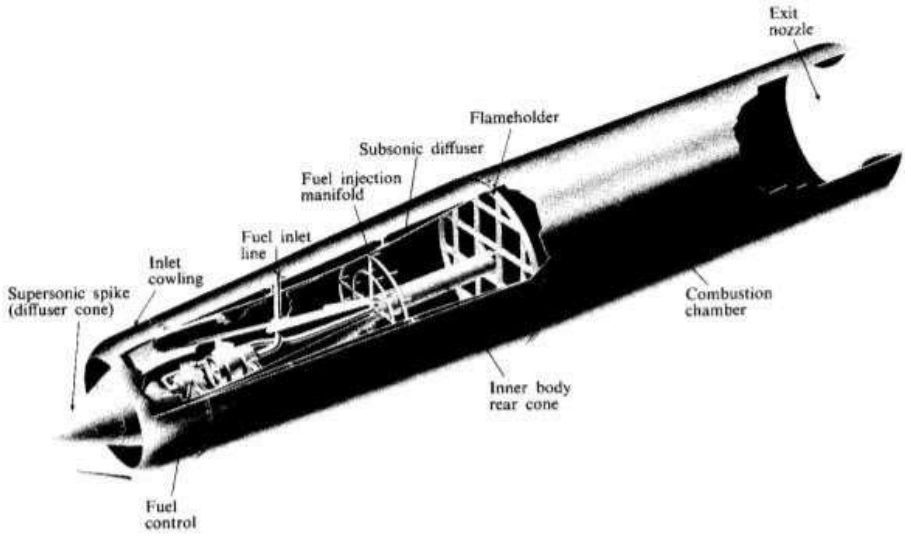

Figure 7. Combustion chamber components.[17]

The figure 7 depicts some parts such as the fuel inlet line, fuel injection manifold, subsonic diffuser, flame holder, fuel control and fuel body rear cone.

The thermal efficiency (n_{th}) of the combustion chamber is influenced by the following mixture parameters and construction details; composition, temperature, and initial mixture velocity; length of the combustion chamber and shape of flame stabilizers [17].

The following issues arise when designing a combustion chamber for a ramjet engine:

a) The stabilization system's design.
b) Injection system selection.
c) The two systems' relative positions.

Before we begin designing the stabilization system, we must first answer the following two questions:

1. What shape should the stabilizer take?
2. What should its coverage and defining dimensions be?

Since the combustion chamber's length depends on the fuel used, we need to investigate the best fuel to be used in our engine.

4.2.1. Jet Engine Fuels

Kerosene blends are used in gas turbine and ramjet engines in aircraft. Kerosene has a high energy content per unit volume and a low vapor pressure, both of which improve drag and altitude performance.

In the United States, standard commercial aircraft jet fuels are designated as Jet A, Jet A-1, and Jet B. Jet A-1 is almost identical to Jet A, with the exception of a lower freezing temperature. In the United States, JP 8 and JP 4 military fuels (where JP stands for jet propellant) are essentially equivalent to Jet A-1 and Jet B, respectively. The international names

for Jet A-1 and Jet B fuel blends are Avtur and Avtag, respectively. Likewise, JP 5 military jet fuel, JP 7, and JP 10 are special kerosene blends designed for high-performance aircraft and missiles, and are also known as Avcat [16].

All of these kerosene blends have very similar net energy content Qf, with the main difference being physical properties such as freezing point. Jet B has a lower freezing point than Jet A-1, allowing it to fly in the stratosphere, where temperatures typically hover around 57°C. However, Jet B has a lower flash point than Jet A-1: 10°C versus 55°C. As a result, because it is much easier to use, Jet A-1 has surpassed Jet B as the preferred general-purpose fuel. Similarly, JP 5 is blended to have a higher flash point than JP 8 (62°C) for improved safety in close quarters, such as aircraft carriers, and is used by the US Navy [16].

Because high-altitude long-range subsonic cruise missiles, such as the air-launched cruise missile (ALCM), have long flight times in the stratosphere, freezing temperature is once again a deciding factor, and JP 10 is blended to have a very low freezing point, 79°C. The JP 7 blend was developed not only to be a fuel, but also to be circulated as a coolant for the supersonic (M=3.3) Lockheed SR-71 Blackbird aircraft's structure, which requires a high heat capacity. Furthermore, the effects of significant frictional heating cause the freezing temperature to rise at supersonic speeds. To meet this requirement, JP 7 is blended with a high flash point of 60°C. This fuel was also employed to power the Boeing X-51 Waverider unmanned scramjet test vehicle that flew at M=5.1 for over 200 s in 2013 [16].

The kerosene blends have the best characteristics for aerospace applications.

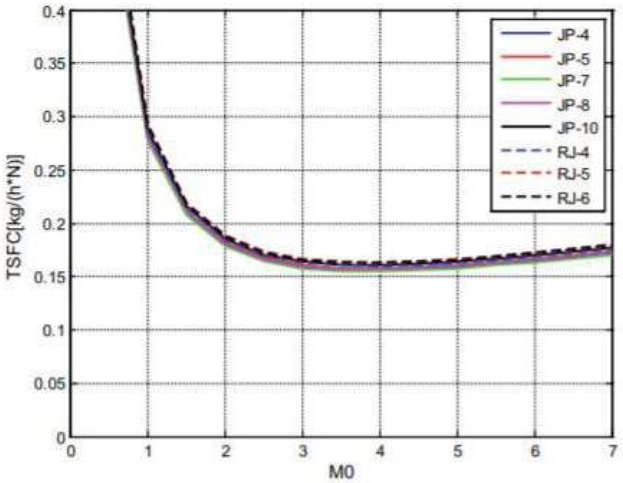

Figure 8. TSFC vs. Mach number for different fuels.[18]

The figure 8 demonstrates the relation between TSFC and Mach number for different fuels.

Table 1. C*, TSFC and mixing ratio of fuel for optimum Mach.[18]

Fuel	C* (m/s)	Ff	TSFC (kg/h/N)
JP-4	1010.44	0.046473	0.165576
JP-5	1011.29	0.046986	0.167261
JP-7	1009.75	0.046060	0.164216
JP-8	1011.08	0.046861	0.166850
JP-10	1013.01	0.048012	0.170624
RJ-4	1012.64	0.047792	0.169904
RJ-5	1014.57	0.048949	0.173685
RJ-6	1014.18	0.048713	0.172915

The table 1 shows the C*, TSFC and mixing ratio of fuel for optimum Mach and some fuel types.

Table 2. Density and reaction heat of some fuels.[18]

Fuel	Density (g/cm^3)	Heating value (MJ/kg)
JP-4	0.76	43,500
JP-5	0.81	43,025
JP-7	0.79	43,890
JP-8	0.81	43,140
JP-10	0.94	42,106
RJ-4	0.93	42,300
RJ-5	1.08	41,300
RJ-6	1.02	41,500

The table 2 depicts the density and reaction heat of some fuels and some fuel types.

4.2.2. Types of Fuel Injectors

There are three types of fuel injectors; parallel, normal and transverse fuel injection.

4.2.2.1. Parallel Fuel Injection

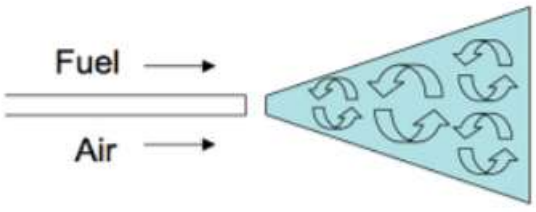

Figure 9. Parallel fuel injection.[19]

In parallel fuel injection in figure 9, fuel flows parallel to the air in the engine but is separated by a splitter plate. A shear layer forms at the splitter plate's end due to the different velocities of the fuel and air.

The shear layer is the primary source of fuel-air mixing, allowing for proper combustion. The shear layer growth rate was reduced compared to theoretical rates when parallel fuel injection with a hydrogen fluorine fuel in the air was tested. The decrease in growth rate is

attributed to a reduction in turbulent shear stress at the core of the shear layer caused by the density change caused by the heat released during the combustion process [19].

4.2.2.2. Normal Fuel Injection

The injection port on the ramjet's wall is used for standard fuel injection. The port delivers fuel to the ramjet in the same direction as the airflow.

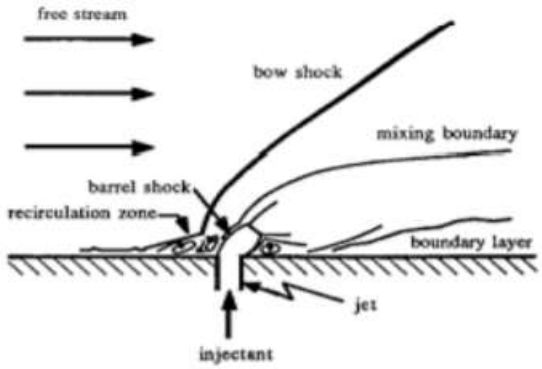

Figure 10. Normal fuel injection.[19]

This injection system produces a detached normal shock upstream of the injector, resulting in separation zones upstream and downstream of the injector, as shown [19].

4.2.2.3. Transverse Fuel Injection

Transverse fuel injection is a cross between parallel and traditional fuel injection. A transverse injector injects fuel at an angle to the flow that is between normal and parallel. Transverse injection addresses some of the shortcomings of conventional injection while necessitating a higher injection pressure to achieve the same penetration height into the airflow. Increased injection pressure increases the scramjet's total pressure loss, lowering engine efficiency [19].

4.2.2.3.1. Strut Injectors

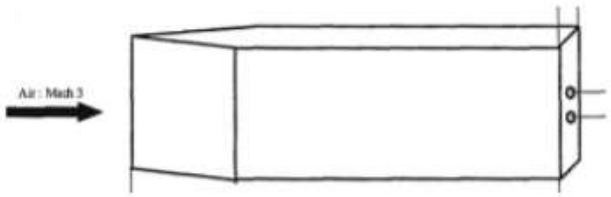

Figure 11. Strut injection.[19]

In figure 11, strut mixing devices are available in a variety of shapes and sizes, and they can be used for both normal and parallel injection. The vast majority of struts are composed of a vertical strut with a wedge leading edge. The strut is linked to both the top and bottom combustion sections. The main advantage of this system is that it allows for uniform radial fuel injection into the core of the airflow. Furthermore, the shock produced by the strut's leading edge improve air-fuel mixing.

The basic strut design was similar in that it was attached to the top and bottom of the test section and had a wedge-shaped leading edge. The designs on the trailing edge, as shown in

Figure 6, were to blame for the disparity. The various trailing edges, referred to as alternating wedge designs, produce either co-rotating or counterrotating vortices, which are used to improve mixing. All of these designs use parallel fuel injection at the strut's trailing edge to entice the fuel into the vortices that cause increased mixing in the combustion section. According to the study's findings, the alternating wedge design produced a more uniform mixing region, but the overall combustion performance is comparable to that of a strut with a flat trailing edge and results in a higher total pressure loss [19].

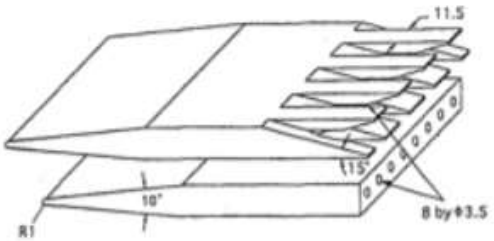

Figure 12. Alternate strut fuel injector.[19].

The figure 12 shows an alternate strut fuel injector.

4.2.2.3.2. Baronage Injection System

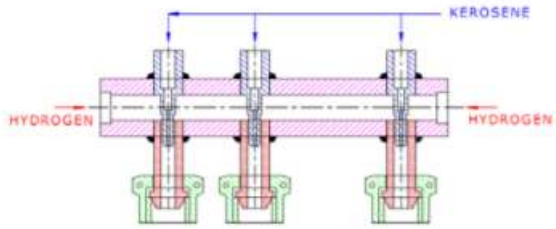

Figure 13. Baronage injector.[19]

The basic configuration of the baronage injection unit is depicted in the figure above. A central tube injects kerosene into the mixing zone, and hydrogen flows through an annular gap around the kerosene tube. In the mixing zone, gas bubbles into the liquid. The two-phase flow is then injected through the injection orifice into the ramjet combustor [19].

4.2.2.3.3. Pulsed Injector

Another type of fuel injection is a conventional pulsed injection, in which fuel is injected as a continuous stream from injection ports into the combustion chamber, where it ignites. This injection method injects fuel in a series of pulses, allowing for greater fuel-air mixing. Combustion happens faster and more efficiently, resulting in more thrust output. The freestream conditions determine the time between pulses, which is coordinated to achieve near stoichiometric combustion.

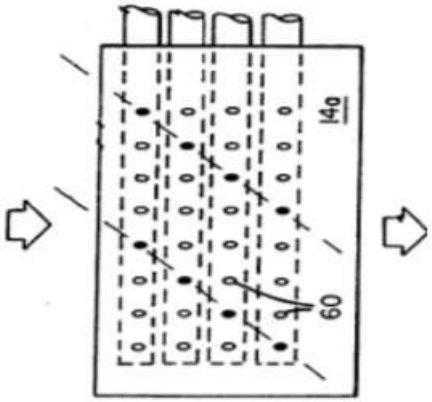

Figure 14. Pulsed injector.[19]

This method has the advantage of always remaining in a transient state and never reaching a steady-state condition. The figure 14 illustrates how to promote fuel-air mixing, a ramjet engine's combustor injects fuel in the form of a series of pulses into the airstream [19].

4.2.3. Positioning of Injectors

They should be placed so that the mixture passing through the flame stabilizer is as close to stoichiometric as possible, as this increases the range of combustion stability. In theory, the distance between the injector and the stabilizer should be chosen so that the fuel in the mixture reaching the stabilizer has already been partially evaporated [18].

4.2.3.1. Flameholders

The intermittent flame initiates combustion, resulting in the formation of a sphere of burned material in the unburned mixture. However, there will be a cone of burned material for the combustion using a continuous spark. The recirculation of hot and burning gases in its wake causes a flame-holding effect on the bluff body. This will serve as an ignition source for the remainder of the mixture. Using a large number of flame holders can shorten the length of the combustion chamber. However, this will result in exorbitant stagnation pressure losses [14].

Increased chamber length increases combustion time, allowing for complete combustion of unevaporated or poorly burned regions. The final design parameter, chamber length, is chosen empirically in order to keep the combustion efficiency above 80 to 90 percent. Flameholders result in drag which reduces stagnation pressures.

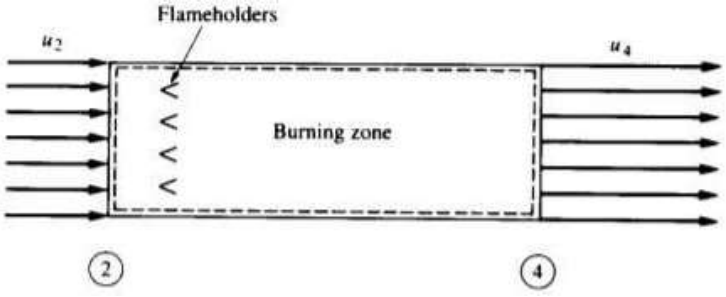

Figure 15. Simplified combustion chamber flow.[14]

The figure above shows that a spider stabilizer improves thermal efficiency in the combustion chamber. It shortens the distance between flames.

4.2.4. Useful Equations in the Combustion Chamber

Energy Balance across the combustor gives:

$$\dot{m}h_{02} + \dot{m}_f Q = (\dot{m} + \dot{m}_f)h_{04} \quad (3)$$

The thrust developed is:

$$F = \dot{m}[(1+f)u_e - u)] \; or \; \frac{F}{\dot{m}} = (1+f)u_e - u \quad (4)$$

$$u_e = u\sqrt{\frac{T_{04}}{T_{0a}}} = u\sqrt{\frac{T_{04}}{T_a}}\sqrt{\frac{1}{1+\frac{\gamma-1}{2}M^2}} \quad (5)$$

The thrust equation can be re-written as

$$\frac{F}{\dot{m}} = M\sqrt{\gamma R T_a}\left[(1+f)\sqrt{\frac{T_{04}}{T_a}}\left(1+\frac{\gamma-1}{2}M^2\right)^{-\frac{1}{2}} - 1\right] \quad (6)$$

$$TSFC = \frac{\dot{m}_F}{F} = \frac{f}{F/\dot{m}_F} \quad (7)$$

4.3. Nozzle

Jet engines have historically powered most military and commercial aircraft. Although turbine engines come in various shapes and sizes, they all have certain characteristics. All gas turbine engines use a nozzle to create thrust, return the exhaust gases to free flow, and regulate the mass flow rate in the engine. The power turbine is located downstream of the nozzle. Compared to other engine parts such as the compressor, it is the primary device [20]. The nozzle is a specially designed part that allows hot gases to pass through it. But it takes some consideration when it comes to arithmetic calculations for the breast. When the Nozzle part is examined for Ramjet, the velocity-area relationship of the nozzle is seen in Figure 1. Speed changes are observed depending on the increase or decrease of the area in the nozzle section. Below the speed of sound, less than Mach 1, the convergent portion of a nozzle accelerates the flow. On the other hand, when the flow is supersonic, greater than Mach 1, the flow from a converging section will slow down in the presence of shocks. A diverging section with increasing area variation will accelerate the flow when the Mach number is greater than 1. This is due to the pressure difference of the supersonic flow where the flow wants to expand, and when it is supersonic, it will accelerate the length of divergence [21].

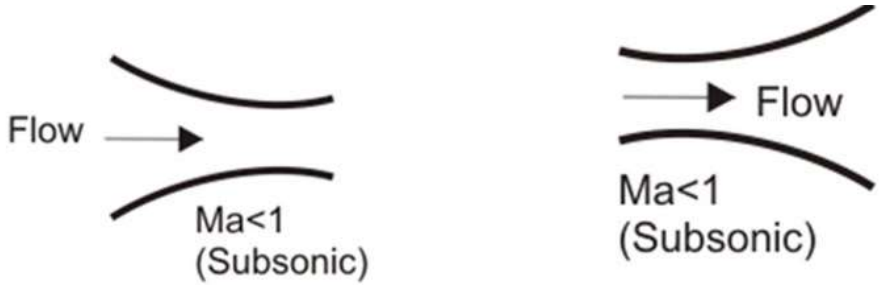

Figure 16. Converging nozzle (left) and Diverging nozzle (right).[21]

For a ramjet engine, there must be a supersonic acceleration of the flow from the nozzle outlet to generate thrust. As shown in figure 16, the nozzle inlet is still subsonic, so the nozzle is designed as a converging-diverging nozzle to achieve supersonic output velocity.

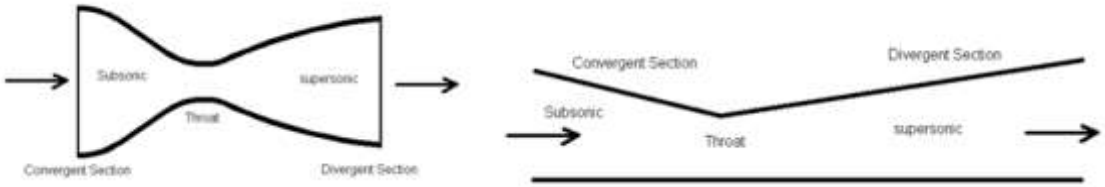

Figure 17. Converging-Diverging Nozzles.[21]

The figure above shows converging-diverging nozzles used as a basis for the design process. The image on the right is more simplistic and reasonable for the scope of this project.

The following section provides detailed information on the influence of geometric configurations on thrust values, along with the design of the propellant nozzle for a ramjet engine for the larger thrust values required, as well as other factors affecting the efficient operation of the nozzle.

4.3.1. Flow Through a Convergent-Divergent (C-D) Nozzle

Compared to the reference reservoir pressure, the ambient pressure for C-D nozzles decreases continuously. However, the flow in the convergent section accelerates until it reaches the sonic velocity (minimum area division) of the throat. The flow does not increase as the ambient pressure is further reduced. However, as the flow approaches the segment leaving the throat, it accelerates to supersonic velocity as indicated by the nozzle. The pressure difference between the outlet and reservoir pressures causes the flow to pass through the nozzle and reach supersonic velocities. Because the region along the convergent portion becomes smaller and the velocity in the throat increases until Mach 1, convergent nozzles are used for flows below Mach 1 (subsonic). A different component follows the joining part at the ConDi nozzle's throat, causing the area to rise instead of contract. If the flow has not yet reached Mach 1, the flow rate will begin to decrease as the retraction increases. If the throat flow (choking flow) reaches Mach 1, the throat area will continue to grow, and the velocity will increase [22].

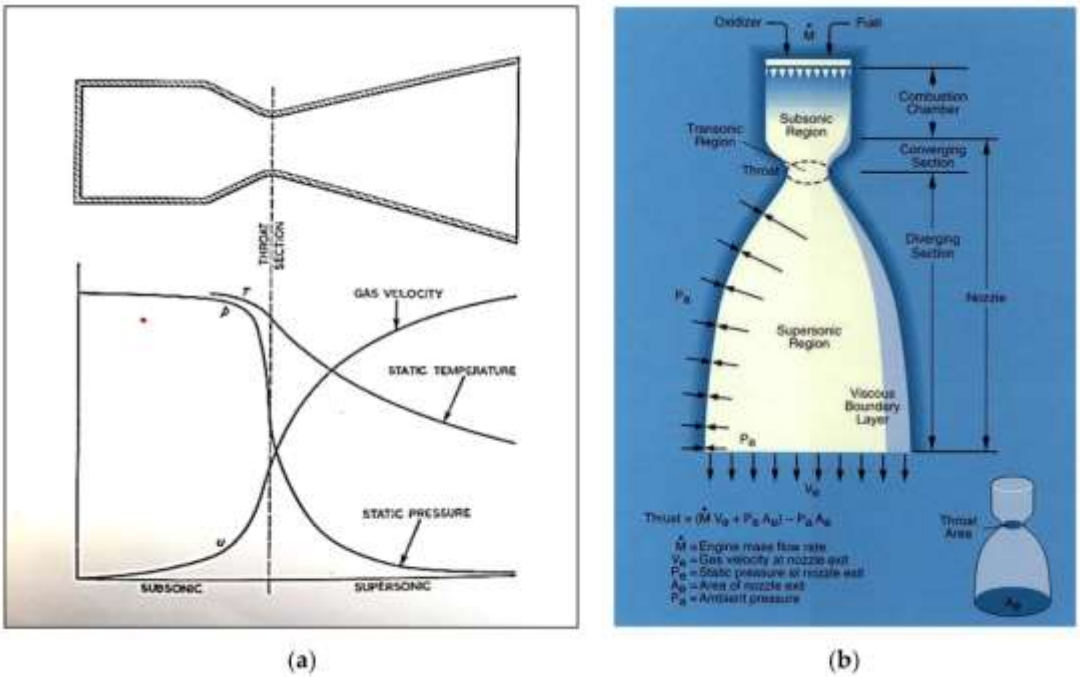

Figure 18. (a) Expansion in a convergent-divergent (C-D) supersonic nozzle and (b) nozzle geometrical designations.[22]

The figure 18-(a) compares gas velocity, static temperature and static pressure from subsonic to supersonic. The figure 18-(b) exhibits how to produce thrust from the convergent-divergent nozzle.

4.3.2. Nozzle Geometric Configurations

The form of the divergent part of the nozzle has traditionally been conical for the simplicity and convenience of production. As the technology progressed and knowledge of aerothermodynamics of convergent-divergent nozzles improved, the classical conical nozzle was replaced by more complex forms to reduce fluid dynamics losses. Other than the conical nozzle, the important ones are Bell Nozzle, Single expansion ramp nozzle, and Annular Nozzles [22].

4.3.2.1. Conical nozzle

The conical nozzle is commonly utilized in rocket applications due to its simplicity and ease of manufacturing. The angle that separates the cross-sectional area of the cone gives it its name. Because the escape velocity axis is maximum at a small angle, the thrust is increased; nevertheless, lowering the angle makes the nozzle longer and heavier, which complicates nozzle formation. A wide nozzle wall angle at the opposite end reduces scale and weight. Unfortunately, broad angles at low altitudes diminish efficiency due to overexpansion and isolation of the flow due to high atmospheric pressure. The escape flow can be done here at any angle that minimizes the vehicle's axial thrust [22].

4.3.2.2. Belli Nozzle

This is the most commonly used nozzle design and has significant size and efficiency advantages over the conical nozzle. Near the throat, the nozzle recedes at a relatively wide angle, but the degree of deviation decreases as the distance from the nozzle increases. The deflection angle at the nozzle outlet is quite modest. In this way, efficiency is increased, and weight is reduced. The most challenging design problem is to shape the nozzle to prevent warping and increase output. However, the bell design will be ideal only at a certain height [22].

4.3.2.3. Single expansion ramp nozzle

Nozzles with single expansion launchers are typically required for hypersonic air-breathing aircraft and rockets where drag is a key criterion. In these nozzles, the lower surface of the nozzle is cut as it causes too much friction compared to the thrust force. The transparent sharp corner positioned at the nozzle inlet provides expansion. This type of nozzle is more effective than the conical nozzle [23].

4.3.2.4. Dual Bell and Contoured Nozzle

The double bell nozzle concept offers a solution to the altitude expansion challenges faced by the traditional bell-shaped nozzles. Contour bending provides a controlled and symmetrical separation; therefore, limiting the occurrence of the split flow of high side loads in conventional nozzles and increasing thrust. The area ratio of the smaller nozzle is relatively smaller than the reference main engine nozzle, resulting in better thrust performance at lower altitudes. The split point detaches from the inflection point on the ascent to higher altitudes. It moves down the ascent plane, where a higher area ratio of the nozzle extension provides thrust with minimal losses from the change in altitude pressure. Double bell nozzles are also classified as altitude compensated nozzles (ACN) [22].

4.3.3. Ramjet Engine Analysis for the Nozzle Section

Considering the outputs from the combustion chamber, this section uses the following equations to close and finalize the model of the Ramjet system. This section gives the final outputs of the system's performance parameters: thrust, outlet Mach, outlet temperature and pressure. The entries in the nozzle analysis section are static temperature, T, stagnation temperature, T_o, static pressure, p, stagnation pressure, p_o, Mach number, M, specific heat ratio after combustion, γ_{hot}, the mass flow of air, $\dot{m}$, inlet velocity, V_1, inlet pressure, p_1, and height and width of the wind tunnel.

Equation (1) can simply calculate the throat area using the cross-sectional area. Based on isentropic relations and ideal gas assumptions, this throat region is necessary to choke the flow [21].

$$\frac{A}{A^*} = \frac{1}{M}\left[\frac{2}{k+1}\left(1+\frac{k-1}{2}M^2\right)\right]^{\frac{k+1}{2(k-1)}} \tag{8}$$

It can be calculated by using Equation (2) with the exit Mach number value and isentropic gas relation to calculate the static exit temperature,

$$T_9 = \frac{T_{t9}}{1+\frac{k-1}{2}M_9^2} \tag{9}$$

The speed of sound at the throat is found using Equation (3),

$$a_8 = \sqrt{(\gamma_{hot} * R_{hot} * T_8)} \tag{10}$$

By using Equation (4) with the exit pressure and rho, the exit Mach number can be calculated,

$$M_9 = \sqrt{\frac{2}{k-1}\left[\left(\frac{p_{t9}}{p_9}\right)^{\frac{k-1}{k}} - 1\right]} \tag{11}$$

Using the static temperature and velocity at the exit can be found by using Equation (5),

$$V_9 = M_9 * a_9 \tag{12}$$

Also, it can be found the exit mass flow rate of the air and fuel mixture in the nozzle throat by using Equation (6),

$$\dot{m}_{air,fuel\,exit} = A^* * a_8 * \rho_8 \tag{13}$$

Using Equation (7), it can be found total pressure at the nozzle exit,

$$p_{t9} = p_{t4} * \pi_n \tag{14}$$

Moreover, to get nozzle total pressure ratio by using Equation (8),

$$\pi_n = \left\{\left(\frac{p_{t4}}{p_9}\right)^{\frac{k-1}{k}} - \eta_n\left[\left(\frac{p_{t4}}{p_9}\right)^{\frac{k-1}{k}} - 1\right]\right\} \tag{15}$$

The thrust of the ramjet engine can be calculated using Equation (9) with the exit pressure, area, mass flow rate and velocity,

$$F = \dot{m}_{air,fuel\,exit} * V_9 - \dot{m}_{air} * V_1 - (p_9 - p_{amb}) * A_9 \tag{16}$$

5. RESULTS AND DISCUSSION

5.1. Engine Design

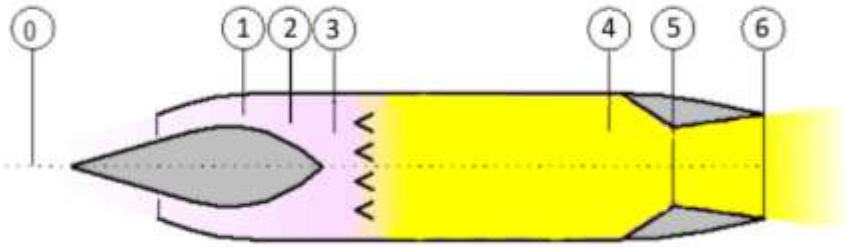

Figure 19. The representative image of our ramjet design.[26]

Throughout this part of the report, it can be seen that explanations about the engine refer to a location inside the engine. The figure 19 shows which location number represents which part of the engine can be seen. One important note is that location 1 is where the normal shock occurs, location 3 is just before the combustion chamber, and location 2 is where the Mach number equals 0.5 between two locations.

The engine design stated with writing a MATLAB code (See appendix A.1). Firstly, there are design parameters which are required from our design. The thrust requirement is 30 kN, and the combustor exit total temperature (location 4) which is required to be at 2000 K. For the design, it is assumed that the nozzle is perfectly expanded. This means two things. First, 30 kN thrust is occurred only due to momentum change. Second, Static pressure at location 6 is equal to location 0.

Secondly, there are some parameters that are known for some reasons. Q_R is fuel heating value. Its value is different in every fuel type. For the design, in the previous parts, it is concluded that Jet-A1 (kerosene) fuel will be the best choice for the design. Jet-A1 has a fuel heating value of 43.15 MJ/kg. C_{p1} and γ_1 values are some properties for air. It is known that air has C_p of 1004.675 J/kg*K and γ of 1.4. Our first assumption is that C_p and γ are constant until the combustion chamber, and new values of C_p and γ after combustion are also constant from the end of combustion until the engine's exit. Although this assumption is not realistic for engine design, this assumption is necessary to calculate some other parameters for the engine. It is also known that in order to make a good design, the Mach number at location 5 must be 1.

Thirdly, some parameters have been assumed. Just before the combustion chamber, the Mach number should be small. Thus, fuel and air can mix more and burn more efficiently. For ramjets, the Mach number at the combustion chamber inlet is generally around 0.3-0.2 [24]. For this reason, M_3 is assumed to be 0.2. For location 2, which is between normal shock and combustion chamber, Mach number is assumed 0.5. This assumption has the same reason with the Mach number assumption at location 3 (M_3) [25]. Moreover, the diameter of the inlet of the combustion chamber is chosen to be 46 cm [26]. Gas constant R is assumed to be constant throughout the engine. Although this is not realistic, it was needed to do it because otherwise, γ_4 has not been found. Instead of C_p or Gamma, R is chosen to be constant because it is known that changes in R values are always the smallest between these three parameters.

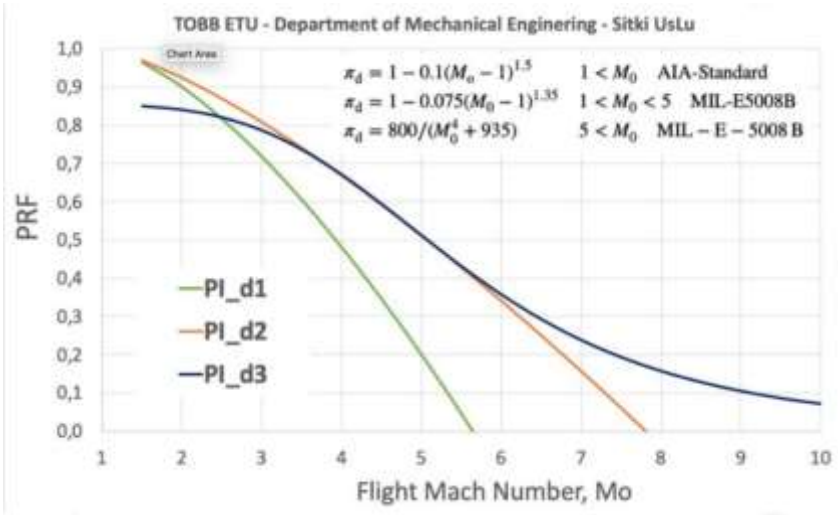

Figure 20. The relation between pressure recovery ratio and flight Mach number.[27]

The chart above shows different assumptions of total pressure losses for different Mach numbers. Before doing an engine inlet design. First, it is needed to find an entry Mach number (M_0), pressure, and temperature value at the chosen altitude. Also, to find M_0, it is needed to have pressure lost to oblique shocks. That is why this chart gathered from experimental data is used at the first iteration. Hence, our first assumption can be found for M_0. By looking at the figure, it is assumed that the total pressure ratio between locations 1 and 0 (P_{t1}/P_{t0}) can be calculated using MIL-E5008B. Although it is said that Mach numbers must be between 2 and 6, because our thrust requirement is relatively low, it is assumed that our Mach number would not be able to pass Mach 5.

For the burner efficiency, fuel-air ratio (f), total pressure ratios between each location (except only location 0 and 1), and total temperature ratios between each location assumptions are based on common values around these types of engines. This is done by looking at some ramjet examples and Gasturb software' demos.

$$\frac{T_t}{T} = 1 + \frac{\gamma-1}{2} M^2 \tag{17}$$

$$\frac{P_t}{P} = (1 + \frac{\gamma-1}{2} M^2)^{\frac{\gamma}{\gamma-1}} \tag{18}$$

This formula above [27] shows the relation between total temperature and pressure and static temperature and pressure. The above relations are widely used in the code (See appendix A.1). The fluid inside the engine is assumed to be ideal. It is also important to note about the code that velocity at location 6 is found from momentum change, Cp at location 4 is found from energy conservation, and Mach number at location 4 is found from solving the choked area relations.

After many iterations of running this first code (See appendix A.1). The first assumptions have been made for M_0 and altitude. Then the second code is written (See appendix A.2). The first purpose of this code is to calculate the total pressure loss between locations 0 and 1 after three oblique shocks. The code does it through taking the shock wave angles as an input.

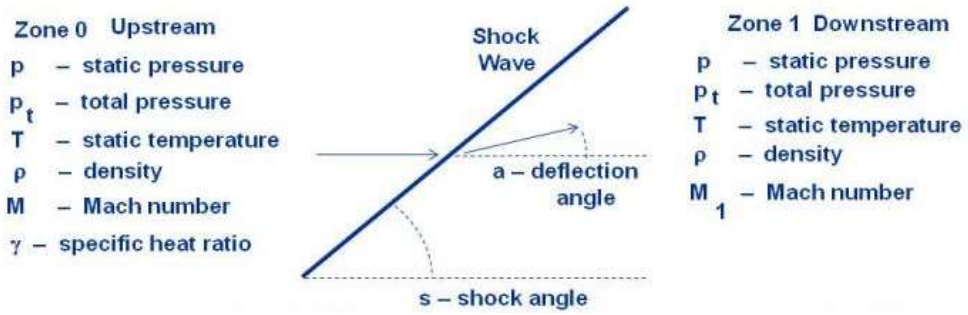

Figure 21. Oblique shock wave.[28]

The figure 21 indicates shock wave, deflection angle and shock angle between zone 0 upstream and zone 1 downstream.

Then, the oblique shock relations calculate the ramp angle, static and total pressure, static temperature, and density after the shock.

$$cota = tans\left[\frac{(\gamma+1)M^2}{2(M^2sin^2s-1)} - 1\right] \tag{19}$$

$$M_1^2sin^2(s-a) = \frac{(\gamma-1)M^2sin^2s+2}{2\gamma M^2sin^2s-(\gamma-1)} \tag{20}$$

$$\frac{T_1}{T_0} = \frac{[2\gamma M^2sin^2s-(\gamma-1)][(\gamma-1)M^2sin^2s+2]}{(\gamma+1)^2M^2sin^2s} \tag{21}$$

$$\frac{P_{t1}}{P_{t0}} = \left[\frac{(\gamma+1)M^2sin^2s}{(\gamma-1)M^2sin^2s+2}\right]^{\frac{\gamma}{\gamma-1}}\left[\frac{(\gamma+1)}{2\gamma M^2sin^2s-(\gamma-1)}\right]^{\frac{1}{\gamma-1}} \tag{22}$$

$$\frac{P_1}{P_0} = \frac{2\gamma M^2sin^2s-(\gamma-1)}{(\gamma+1)} \tag{23}$$

$$\frac{\rho_1}{\rho_0} = \frac{(\gamma+1)M^2sin^2s}{(\gamma-1)M^2sin^2s+2} \tag{24}$$

The oblique shock relations which are used in the second code are shown above [28]. 3 number of ramps are chosen for this design. This is because the Mach number at around 3 is relatively low from scramjets, which usually have five ramps. Hence, it is considered that five ramps would be too much for our design, and then three ramps have been decided for our design.

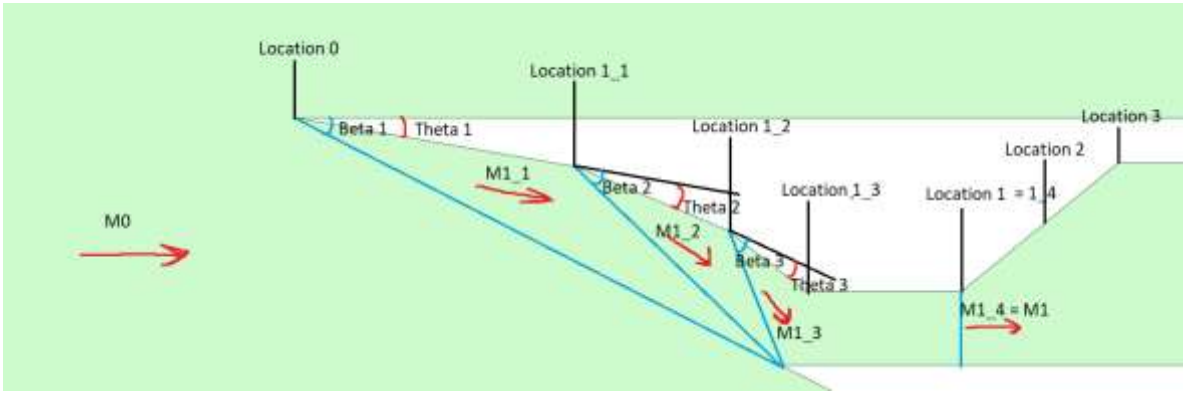

Figure 22. Engine inlet design.[30]

The figure above shows our engine inlet design. Locations, wave and ramp angles, and Mach numbers can be seen from this figure. The white area represents the engine inlet, and the green area is the air. It is also important to see that all the wave angles clash at the same point where the bottom part of the inlet ends. Also, normal shock occurs at the end of the throat.

Table 3. The value of each parameter at each location between locations 0 and 1 of the engine.

	Units	Loc. 0	Loc. 1_1	Loc. 1_2	Loc. 1_3	Loc. 1_4
Beta Angle	deg	27.1	34.4	45.6	-	90
Theta Angle	deg	9.9230	12.9617	14.9892	-	0
Mach no.	-	3.03	2.5333	1.9888	1.4357	0.7252
Density	kg/m^3	0.2171	0.3594	0.6266	1.0816	1.8943
Static P.	kPa	13.5	27.757	61.710	135.08	302.31
Total P.	kPa	518.68	499.47	474.53	452.13	429.00
Static T.	K	216.65	269.0809	343.0659	435.0980	555.9853

After various iterations to find the minimum pressure loss with changing shock angles. The results are gathered from the code are shown in the table above. The table 3 exhibits the value of each parameter at each location between locations 0 and 1 of the engine. In the end, the Total Pressure Ratio (TPR) of our inlet design is calculated as 429.00/518.68 = 0.8271.

These two MATLAB codes also run together to find the optimum values for the design. After many iterations, our Mach number (M_0) is concluded to be 3.03, and our altitude is concluded to be 14275 meters. At that altitude, the temperature is 216.65 K, and the pressure is 13.5 kPa.

Table 4. The results of whole engine performance calculations.

	Units	Loc. 0	Loc. 1	Loc. 2	Loc. 3	Loc. 4	Loc. 5	Loc. 6
Mass Flow Rate	kg/s	36.5296	36.5296	36.5296	36.5296	38.2100	38.2100	38.2100
Area (A)	m^2	0.1882	0.0563	0.0725	0.1662	0.1662	0.1184	0.4473
Velocity	m/s	894.0561	342.7723	250.0259	102.5869	402.7395	814.8904	1639.9
Speed of Sound (a)	m/s	295.0680	472.6879	500.0518	512.9343	852.0940	814.8904	612.8874
Mach Number	-	3.03	0.7252	0.5	0.2	0.4726	1	2.6757
Density	kg/m^3	0.2171	1.8943	2.0147	2.1426	0.5945	0.3962	0.0521
Gamma	-	1.4	1.4	1.4	1.4	1.3082	1.3082	1.3082
Cp	J/kg*K	1004.7	1004.7	1004.7	1004.7	1218.3	1218.3	1218.3
Fuel-Air Ratio (f)	-	0	0	0	0	0.046	0.046	0.046
Static Pressure	kPa	13.5	302.31	359.85	402.66	329.95	201.10	149.56
Total Pressure	kPa	518.68	429.00	426.86	414.05	380.93	369.50	351.02
Total Enthalpy	kJ	617.33	649.82	656.39	663.02	2436.6	2486.3	2563.2
Total Entropy	kJ/K	2.6735	2.7795	2.7910	2.8099	5.5714	5.6048	5.6566
Static Temperature	K	216.65	555.9853	622.2206	654.6934	1933.4	1768.3	1000.3
Total Temperature	K	614.4584	646.7983	653.3316	659.9309	2000	2040.8	2103.9

The table 4 indicates the actual results from MATLAB. The engine's specific thrust is 821.2520 m/s, the fuel-specific impulse is 1819.9 s, Thrust Specific Fuel Consumption (TSFC) is 56.0120 g/kN*s, propulsion efficiency (n_p) is 72.93%, thermal efficiency (n_{th}) is 53.39%, and overall efficiency is 38.94%.

5.2. Analysis of Important Parameters

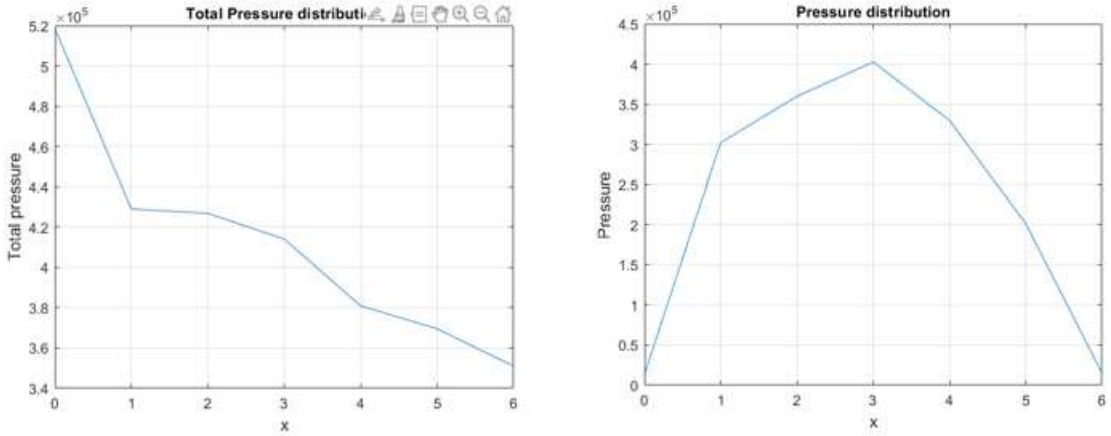

Figure 23. The total pressure distribution (left) and pressure distribution (right) relations.[29]

Here there are two graphs shown above. The left graph is about the total pressure distribution throughout the engine. The left graph shows the total pressure of fluid at each location. The right chart is about static pressure distribution throughout the engine. Static pressure of the fluid at each location can be seen from the graph at the right.

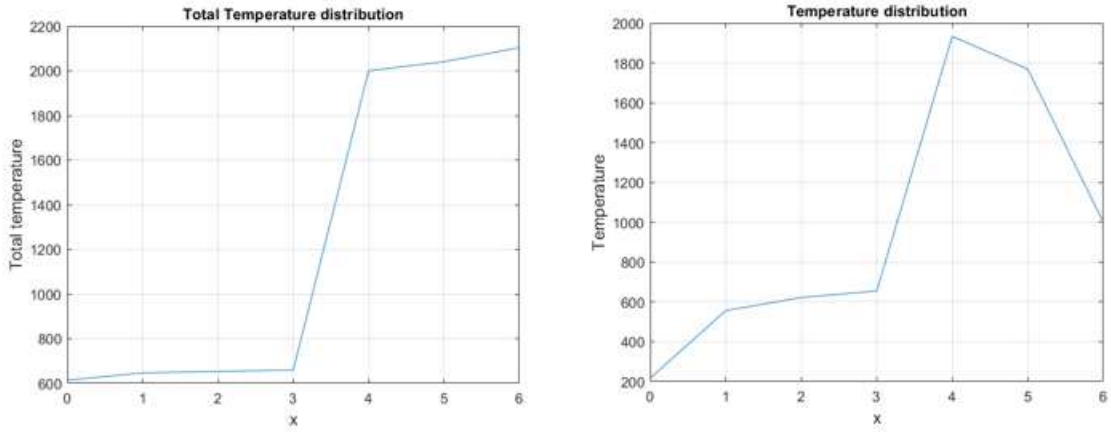

Figure 24. The total temperature distribution (left) and temperature distribution (right) relations.[29]

Here there are two graphs shown above. The left graph is about the total temperature distribution throughout the engine. The left graph shows the total temperature of fluid at each location. The right chart is about static temperature distribution throughout the engine. The static temperature of the fluid at each location can be seen from the graph at the right.

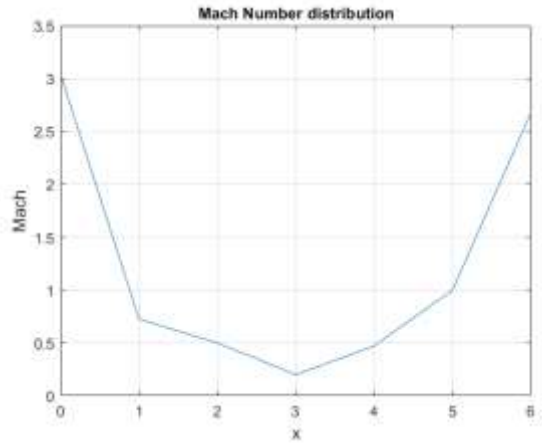

Figure 25. The relation between Mach number distribution and the location of each stage.[29]

The graph 25 is about Mach Number distribution throughout the engine. Mach number of fluid at each location can be seen by looking at this graph.

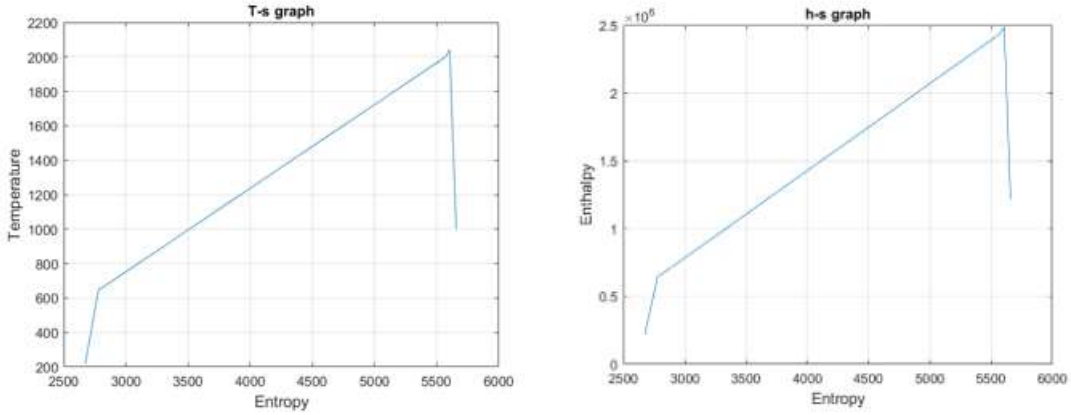

*Figure 26.*Temperature and enthalpy relation with entropy.[29]

Here there are two more graphs shown above. The left graph is about temperature vs. entropy at each stage of the engine. The temperature and entropy of the fluid at each stage can be seen from the left graph. The right graph is about enthalpy vs. entropy at each stage of the engine. Enthalpy and entropy of the fluid at each stage can be seen from the graph at the right. These two graphs also show that the engine is a real engine, not an ideal engine. This is because entropy is always increasing from stages 0 to 2 and 4 to 6.

5.3. The Analysis of Engine Performance and Comparison

Table 5. The results of the GasTurb 14 software.[26]

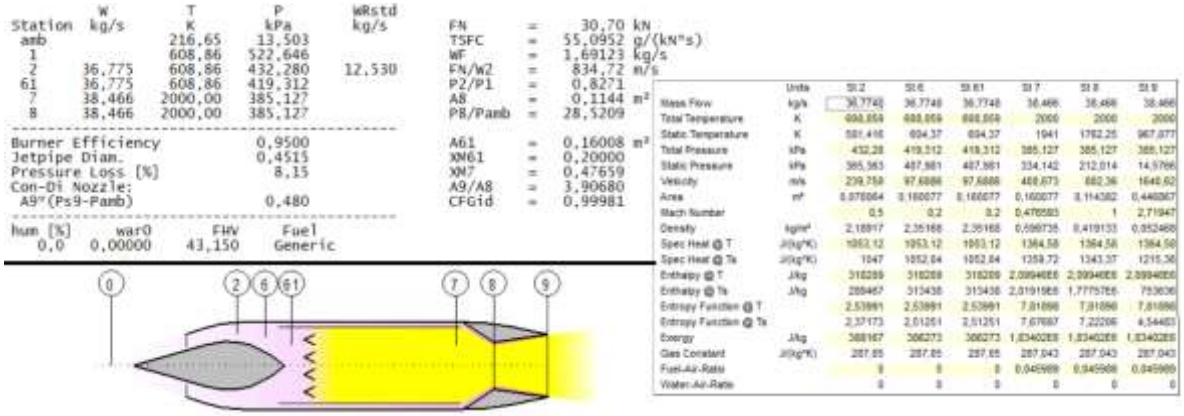

Station	W kg/s	T K	P kPa	WRstd kg/s
amb		216,65	13,503	
1		608,86	522,646	
2	36,775	608,86	432,280	12,530
61	36,775	608,86	419,312	
7	38,466	2000,00	385,127	
8	38,466	2000,00	385,127	

Burner Efficiency		0,9500	
Jetpipe Diam.		0,4515	
Pressure Loss [%]		8,15	
Con-Di Nozzle:			
A9*(Ps9-Pamb)		0,480	

hum [%]	war0	FHV	Fuel
0,0	0,00000	43,150	Generic

FN	=	30,70	kN
TSFC	=	55,0952	g/(kN*s)
WF	=	1,69123	kg/s
FN/W2	=	834,72	m/s
P2/P1	=	0,8271	
A8	=	0,1144	m²
P8/Pamb	=	28,5209	
A61	=	0,16008	m²
XN61	=	0,20000	
XN7	=	0,47659	
A9/A8	=	3,90680	
CFGid	=	0,99981	

	Units	St.2	St.6	St.61	St.7	St.8	St.9
Mass Flow	kg/s	36,7748	36,7748	36,7748	38,466	38,466	38,466
Total Temperature	K	608,859	608,859	608,859	2000	2000	2000
Static Temperature	K	581,416	604,37	604,37	1941	1782,25	967,877
Total Pressure	kPa	432,28	419,312	419,312	385,127	385,127	385,127
Static Pressure	kPa	365,363	407,881	407,881	334,142	212,014	14,5766
Velocity	m/s	239,759	97,6886	97,6886	488,673	682,36	1640,62
Area	m²	0,070864	0,160077	0,160077	0,160077	0,114382	0,446067
Mach Number		0,5	0,2	0,2	0,476583	1	2,71947
Density	kg/m³	2,18917	2,35168	2,35168	0,669735	0,419133	0,052466
Spec Heat @ T	J/(kg*K)	1053,12	1053,12	1053,12	1364,58	1364,58	1364,58
Spec Heat @ Ts	J/(kg*K)	1047	1052,84	1052,84	1359,72	1343,37	1215,36
Enthalpy @ T	J/kg	318289	318289	318289	2,0994E6	2,0994E6	2,0994E6
Enthalpy @ Ts	J/kg	288467	313438	313438	2,0191E6	1,7775E6	753636
Entropy Function @ T		2,53991	2,53991	2,53991	7,01896	7,01896	7,01896
Entropy Function @ Ts		2,37173	2,51251	2,51251	7,07697	7,22206	6,54483
Energy	J/kg	388167	306273	306273	1,8346E6	1,8346E6	1,8346E6
Gas Constant	J/(kg*K)	287,05	287,05	287,05	287,043	287,043	287,043
Fuel-Air-Ratio		0	0	0	0,045989	0,045989	0,045989
Water-Air-Ratio		0	0	0	0	0	0

The engine design is tested on GasTurb 14. The results from here can be compared to the table created by the results of the MATLAB code. It can be seen that our MATLAB code is consistent with the Gasturb results. However, there are small differences in some of the values. This is normal because of the different assumptions that have been made from MATLAB. In our code, temperature and pressure losses have been added between every location. However, Gasturb assumes no total temperature loss through the engine and no pressure loss at the nozzle. For example, the code has pressure loss at the nozzle, but at the end of the nozzle, static pressure equals the atmospheric pressure, so it results in a perfect expansion. However, when using values in MATLAB, it can be seen overexpansion at the end of the nozzle, so because of that, there is about 0.5 kN more thrust in the Gasturb. This is one example of different assumptions. If the MATLAB assumptions could be the same with the Gasturb data, the results could be exactly the same.

6. COMPUTATIONAL FLUID DYNAMICS (CFD) RESULTS

6.1. Inlet Design

For the inlet design, a rectangular inlet shape is used. The area at each location is known so, only the width of the inlet is decided as 0.28 m. After the inlet, the engine becomes circular with a diameter of 46 cm. The CFD analysis is done on Ansys software.

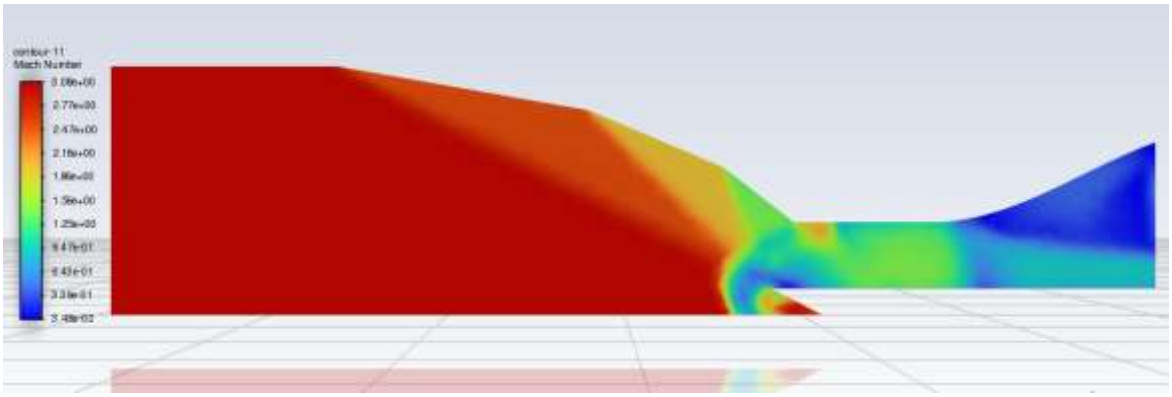

Figure 27. Mach number distribution for the inlet.[30]

The figure 27 shows the Mach number distribution through the engine inlet. It can be seen that three oblique shocks are occurred with right wave angles. As expected, the normal shock has also occurred at the end of the throat. The expected Mach number values are also consistent. However, there are some small unexpectancies. At the tip of the bottom wall, there seems to be a bow shock created, and after the normal shock fluid, it does not mix well. This may be due to Ansys' no total pressure and total temperature loss assumption different from ours.

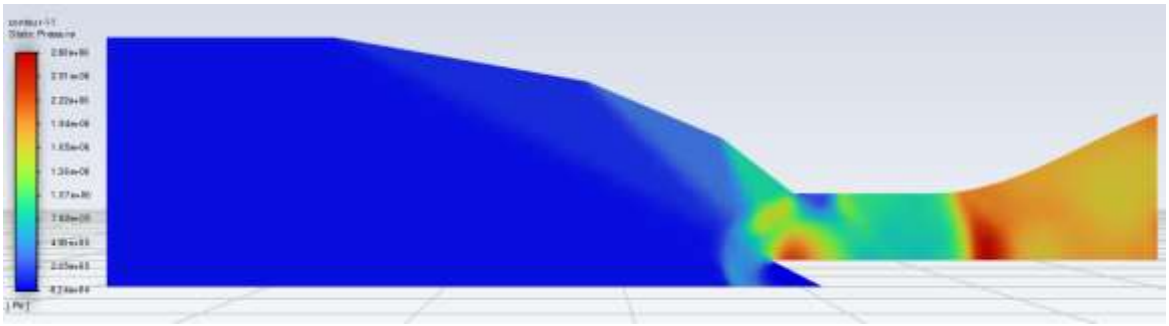

Figure 28. Static Pressure distribution for the inlet.[30]

The figure 28 depicts the Static Pressure distribution through the inlet. As it is said for the Mach number distribution figure, the same things can be said for this figure as well. The software inputs and outputs gauge pressure values about the pressure figure in Ansys. This means that the figure above shows the pressure value without adding atmospheric pressure (13.5 kPa). When it is added, it can be seen the values are also consistent. Normal shock is more visible in this figure, and this figure shows the fluid after the normal shock is mixed more.

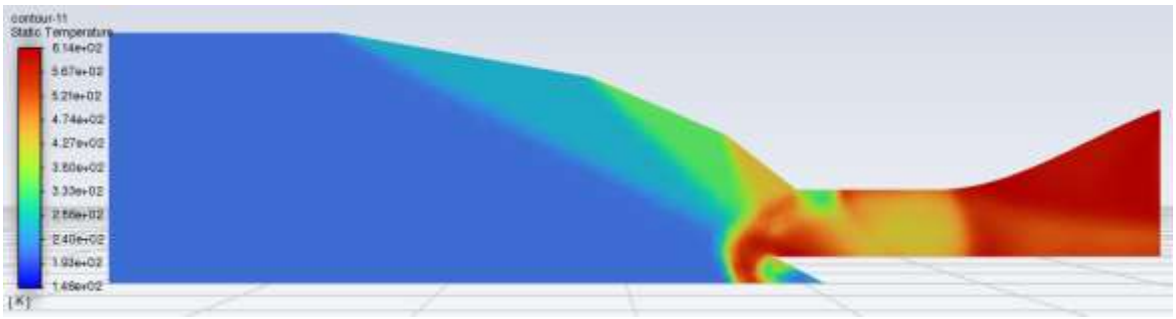

Figure 29. Static Temperature distribution for the inlet.[30]

The figure 29 is about static temperature distribution through the inlet. Also, the same things can be said about this figure. The values are also consistent. Normal shock and after that is more visible in this one as well.

6.2. Nozzle Design

For the nozzle design, the areas are known, and the geometry is cylindrical. So, height is also known.

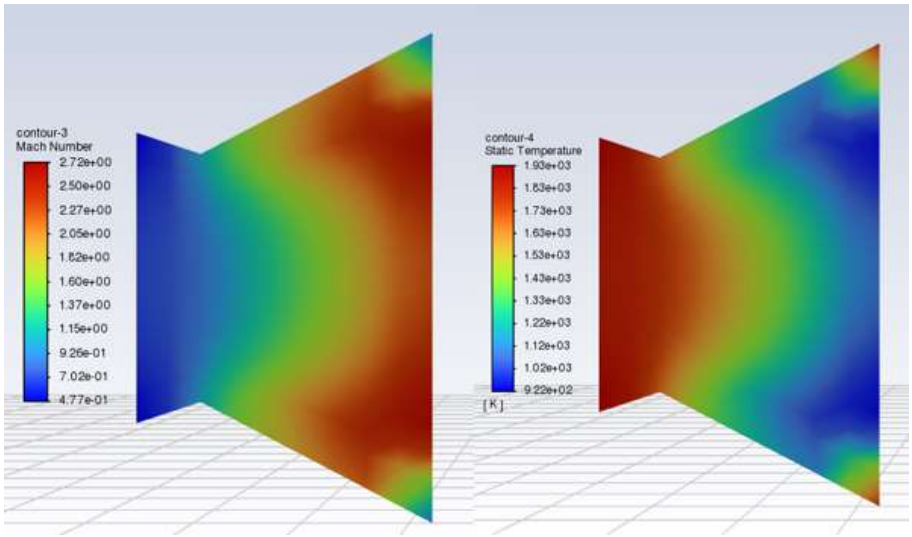

Figure 30. Mach number distribution (left) and static temperature distribution (right) for the nozzle.[30]

Here there are two figures that can be seen above. The left figure is about Mach number distribution through the nozzle. It can be said that normal shock occurs at the chock point as expected. Also, the Mach number increases until 2.72 at the end, which is consistent. However, like the inlet, this has some small differences. It can be seen an under expansion at the edges. This may also be caused by different assumptions between the code and Ansys. The right figure is about static temperature distribution through the nozzle. Very much the same things can be said about this figure like the left one as well.

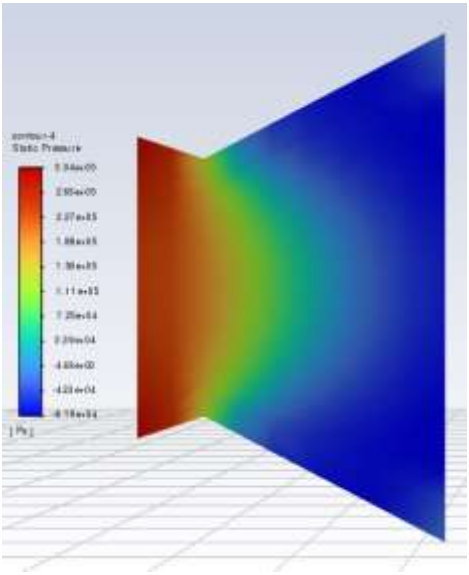

Figure 31. Static Pressure distribution for the nozzle.[30]

The figure 31 demonstrates the static pressure distribution through the nozzle. The same comments can be made for this figure as well, like the previous Mach number and static pressure distribution figures. Like the inlet parts pressure distribution figure, this figure also shows the values without adding the atmospheric pressure as well. So, when it is added, values are also consistent with minor differences caused by different assumptions.

7. CONCLUSION

Internal compression, external compression, and mixed compression are the three primary types of intake models defined by the supersonic compression wave system. Furthermore, due to differences such as supersonic and subsonic flows, developing and sizing a supersonic intake is more complicated than designing and sizing a subsonic inlet. Also, the two most important performance criteria for supersonic inlets are total pressure recovery and flow distortion.

In combustors, a spider stabilizer is used to improve thermal efficiency in the combustion chamber. The length of the combustion chamber is determined by the type of fuel used, the injector and the flame holder characteristics. The Jet A1 or JP 8 engine fuel has been chosen because it is much easier to handle than Jet B. It has a heating value of 43140 MJ/kg and a total specific heat capacity of 0.166850 kg/h/N. After much consideration, the strut injector was chosen as it allows fuel to be injected into the core of the airflow with uniform radial spreading. In place of the intermittent spark, a continuous spark was chosen. In contrast, the intermittent spark produces a sphere of burned and unburnt material. Flameholders are highly recommended to reduce stagnation pressure losses and keep the flame stable. A bluff body has added the benefit of creating a flame-holding effect, which acts as the ignition for the rest of the mixture.

The most preferred nozzle design for ramjet is the convergent-divergent design. The main reason for this is that the ramjet travels at supersonic speeds and is most efficient with Mach values between 3 and 6. Therefore, the ConDi nozzle is used in this project design. Mach value was calculated as $A_9/A_8 = 3.908$ using GasTurb14 and MATLAB code. In addition, the throat area is calculated as 0.1144 m^2 and the inlet nozzle as 0.16008 m^2.

In the results and discussion part, some assumptions have been made and combined with the known facts to achieve our goals (30 kN thrust and 2000 K T_{04}). Put them all into a MATLAB code to calculate all the important parameters at every point of the engine. A second code is written using the oblique shock relations to find these parameters for the engine inlet part. The perfect Mach number and altitude are found working on these codes together. After many iterations, it is concluded that M_0=3.03 and altitude at 14275 meters are best for our design, and other values were found accordingly. Also, running these codes at this Mach number and altitude gave us these important parameters at every stage of the engine. These values are compared with the values from GasTurb 14 software, and they are consistent with minor errors caused by different assumptions that have been made and GasTurb uses. In the end, our engine's performance can be seen from the following values; specific thrust is 821.2520 m/s, fuel specific impulse is 1819.9 s, TSFC is 56.0120 g/kN*s, propulsive efficiency is 72.93%, thermal efficiency is 53.39%, and overall efficiency is 38.94%. Moreover, with the values taken from the MATLAB code, CFD analysis is done on engine inlet and nozzle parts by the Ansys software. It can be seen that our oblique shock angles, Mach number, temperature and pressure after each shock, and the location of normal shock are very consistent with the code.

For future work, experimental data can be gathered from the field tests by building the engine physically. New data collected from the experiments can be implemented into code so that some geometries can be redone in the next iteration. Especially, new total pressure and total temperature ratios are likely to be much better than the values assumed in the code so, this would change the engine's performance in a good way.

REFERENCES

[1] *"Ramjet / Scramjet thrust"* (2015, May 5). NASA Glenn Research Center. Retrieved from: https://www.grc.nasa.gov/www/k-12/airplane/ramth.html.

[2] "*What is a Ramjet?"* (2022, February 3). wiseGEEK: clear answers for common questions. Retrieved from: https://www.wise-geek.com/what-is-a-ramjet.htm.

[3]*"Ramjet*" (2001, December 3). Wikipedia, the free encyclopedia. Retrieved February 3, 2022, from: https://en.wikipedia.org/wiki/Ramjet.

[4] Trevor English. (2020, December 11). "*The history and development of hypersonic flight*". Interesting Engineering. Retrieved from: https://interestingengineering.com/the-history-and-development-of-hypersonic-flight.

[5] El-Sayed, A. F. (2016). *Fundamentals of aircraft and rocket propulsion* (1st ed., Vols., pp. 338–341). Springer.

[6]"Leduc 0.10 Le Bourget 2007.jpg" (2020, September 17). Wikimedia Commons, the free media repository. Retrieved January 29, 2022 from: http://www.aviastar.org/pictures/france/leduc_010.jpg.

[7]"*Ramjet operation*" (2021, August 23). Wikimedia Commons. Retrieved February 3, 2022, from: https://commons.wikimedia.org/w/index.php?title=File:Ramjet_operation.svg&oldid=584634456.

[8] El-Sayed, A. F. (2016). *Fundamentals of aircraft and rocket propulsion* (1st ed., Vols., pp. 342–346). Springer.

[9] Mattingly, J. D. (1995). *Elements of gas turbine propulsion*. McGraw-Hill Science, Engineering & Mathematics, pp. 776-790.

[10] *Inlets.* (2020). ACS College Of Engineering - Mysore Road in Bangalore. Retrieved from: https://www.acsce.edu.in/acsce/wp-content/uploads/2020/03/Module-3-18AE43.pdf.

[11] *Fluid flow studies of the F-5E and F-16 inlet ducts | NTU Singapore*. (2008). Digital Object Identifier System. Retrieved from: https://doi.org/10.32657/10356/14581.

[12] *Design and analysis of an air intake system of Ramjet engine using CFD simulations.* (2021). ResearchGate. Retrieved from: https://www.researchgate.net/publication/349694971_Design_and_Analysis_of_an_Air_Intake_System_of_Ramjet_Engine_Using_CFD_Simulations.

[13] Hill, P. G., & Peterson, C. R. (1992). *Mechanics and thermodynamics of propulsion*. Pearson.

[14] ASE 435 Propulsion Systems II – Ramjet, Lecture Notes. Middle East Technical University Northern Cyprus Campus, 2022.

[15] Dugger, G. L., “Recent Advances in Ramjet Combustion” (2018). ARS Journal ol. 29, No. 11, 195.

[16] *Ramjet engines*. (2020). ScienceDirect.com | Science, health and medical journals, full text articles and books. Retrieved from: https://www.sciencedirect.com/topics/engineering/ramjet-engines.

[17] Pasquale M. Sforza. (2017). *Theory of aerospace propulsion (Second Edition)*. Butterworth-Heinemann.

[18] Ingenito, A. (2021). *Subsonic combustion Ramjet design*. Springer.

[19] Anjali PateL, Gopal Sahu, Prakash Kumar Sen. (2015). A Review on Fuel Injection System of Scramjet Engine. *International Journal of Engineering and Management Research*, *5*(5), 199-202. Retrieved from: https://www.ijemr.net/DOC/AreviewOnFuelInjectionSystemOfScramjetEngine(199-202).pdf.

[20] “*Engines”* (2021, May 13). NASA Glenn Research Center. Retrieved from: https://www.grc.nasa.gov/www/k-12/UEET/StudentSite/engines.html.

[21] *Nozzle Design for the Supersonic Wind Tunnel Ramjet Attachment*. (2013, June). DigitalCommons@CalPoly | California Polytechnic State University, San Luis Obispo Research. Retrieved from: https://digitalcommons.calpoly.edu/cgi/viewcontent.cgi?article=1127&context=aerosp.

[22] *Ramjet Nozzle Analysis for Transport Aircraft Configuration for Sustained Hypersonic Flight*. (2018). MDPI - Publisher of Open Access Journals. Retrieved from: https://res.mdpi.com/d_attachment/applsci/applsci-08-00574/article_deploy/applsci-08-00574.pdf.

[23] *“Sern*” (2005, October 9). Wikipedia, the free encyclopedia. Retrieved February 2, 2022, from: https://en.wikipedia.org/w/index.php?title=SERN&oldid=960779008.

[24] Ceglie, V., Capurso, T., Oresta, P., & Camporeale, S. M. (2020). Analysis of the influence of the mean flow Field Mach number on thermo-acoustic combustion instability. *E3S Web of Conferences*, *197*, 11004. Retrieved from: https://doi.org/10.1051/e3sconf/202019711004.

[25] *Ramjets and scramjets*. (2003). ScienceDirect.com | Science, health and medical journals, full text articles and books. Retrieved from: https://www.sciencedirect.com/science/article/pii/B0122274105009091.

[26] GmbH, G. (2020). GasTurb 14. Retrieved from: https://www.gasturb.de/.

[27] ASE 435 Propulsion Systems II – Ramjet, Lecture Notes. Middle East Technical University Northern Cyprus Campus, 2022.

[28] “*Oblique shock waves”* (2021, May 13). NASA Glenn Research Center. Retrieved from: https://www.grc.nasa.gov/www/k-12/airplane/oblique.html.

[29] The Math Works, Inc. MATLAB. Version 2021b, The Math Works, Inc., 2022. Computer Software. Retrieved from: www.mathworks.com/.

[30] Ansys. Academic Research Mechanical, (2022). Release 18.1, Help System, Coupled Field Analysis Guide, ANSYS, Inc. Retrieved from: https://www.ansys.com/products/fluids.

[31] ASE 435 Propulsion Systems II, Development of a Ramjet Engine Design Code and CFD Analysis of Engine Intake for the Design Point Mach Number, Project Manual. Middle East Technical University Northern Cyprus Campus, 2022.

APPENDICES

A) MATLAB Codes

A.1. Ramjet Engine

```
clear
clc

%Changing parameters
M0 = 3.03;              %inlet mach number
T0 = 216.65;            %K at 14275 m
P0 = 13500;             %Pa at 14275 m

%Known parameters
Qr = 43150000;          %Fuel Heating value of Jet A1(kerosene) (J/kg)
Cp1 = 1004.675;         %Cp of air (J/Kg*K)
gamma1 = 1.4;           %gamma of air (Cp/Cv)
Tt4 = 2000;             %total temperature after combustion
T = 30000;              %Net Thrust (N)
M5 = 1;                 %choke point of con-di nozzle

%Assumptions
M2 = 0.5;               %mach number at location 2
A3 = pi*(0.46/2)^2;     %area at combustion inlet
M3 = 0.2;               %mach number at combustion inlet
Pt1_Pt0 = 0.8271;       %inlet total pressure loss(found in other code)
%(1-(0.075*(M0-1)^(1.35)) is used for first iteration of Pt1_Pt0
Pt2_Pt0 = Pt1_Pt0*0.995;    %locatioon between 1 and 3 which has Mach 0.5
Pt3_Pt2 = 0.97;         %diffuser total pressure loss
Pt4_Pt3 = 0.92;         %burner total pressure loss
Pt5_Pt4 = 0.97;         %nozzle total pressure loss (convergent part)
Pt6_Pt5 = 0.95;         %nozzle total pressure loss (divergent part)
Tt0_Tt1 = 0.95;         %total temperature ratios through the engine
Tt1_Tt2 = 0.99;
Tt2_Tt3 = 0.99;
Tt4_Tt5 = 0.98;
Tt5_Tt6 = 0.97;
b_eff = 0.95;           %burner efficiency
f = 0.046;              %fuel/air ratio

R = Cp1*(gamma1-1)/gamma1;

%At location 0 (inlet)
Tt0 = T0*(1+(gamma1-1)/2*M0^2);
Pt0 = P0*(1+(gamma1-1)/2*M0^2)^(gamma1/(gamma1-1));
a0 = sqrt(gamma1*R*T0);
V0 = a0*M0;
rho0 = P0/(R*T0);

%At location 2 (after the end of engine inlet)
Tt2 = Tt0/(Tt0_Tt1*Tt1_Tt2);
T2 = Tt2/(1+(gamma1-1)/2*M2^2);
Pt2 = Pt0*Pt2_Pt0;
P2 = Pt2/(1+(gamma1-1)/2*M2^2)^(gamma1/(gamma1-1));
```

```
a2 = sqrt(gamma1*R*T2);
V2 = a2*M2;
rho2 = P2/(R*T2);

%At location 3 (just before combustion chamber)
Tt3 = Tt2/(Tt2_Tt3);
T3 = Tt3/(1+(gamma1-1)/2*M3^2);
Pt3 = Pt2*Pt3_Pt2;
P3 = Pt3/(1+(gamma1-1)/2*M3^2)^(gamma1/(gamma1-1));
a3 = sqrt(gamma1*R*T3);
V3 = a3*M3;
rho3 = P3/(R*T3);

%some important calculations
m_a = A3*rho3*V3;          %air flow rate
m_f = f*m_a;               %fuel flow rate
m_t = m_a + m_f;           %total flow rate
A2 = A3*rho3*V3/(rho2*V2);  %area at location 2
A0 = A2*rho2*V2/(rho0*V0);  %area at location 0
V6 = (T+(m_a*V0))/m_t;      %velocity at the exit of nozzle
Cp4 = ( (Qr*m_f*b_eff)+(m_a*Cp1*Tt3) ) / (m_t*Tt4);   %energy conservation
gamma4 = Cp4/(Cp4-R);       %gamma after combustion

%At location 6 (end of nozzle)
Tt6 = Tt4/(Tt4_Tt5*Tt5_Tt6);
T6 = Tt6 - (V6^2)/(2*Cp4);
a6 = sqrt(gamma4*R*T6);
M6 = V6/a6;
Pt6 = Pt3*Pt4_Pt3*Pt5_Pt4*Pt6_Pt5;
P6 = Pt6/(1+(gamma4-1)/2*M6^2)^(gamma4/(gamma4-1));
rho6 = P6/(R*T6);
A6 = m_t/(rho6*V6);

%At location 5 (choke point of nozzle)
Tt5 = Tt4/(Tt4_Tt5);
T5 = Tt5/(1+(gamma4-1)/2*M5^2);
a5 = sqrt(gamma4*R*T5);
Pt5 = Pt3*Pt4_Pt3*Pt5_Pt4;
P5 = Pt5/(1+(gamma4-1)/2*M5^2)^(gamma4/(gamma4-1));
V5 = a5*M5;
rho5 = P5/(R*T5);
A5 = m_t/(rho5*V5);

%At location 4 (just before nozzle)
A4 = A3;
   %Find M4 by solving choked area ratio vs Mach number relations
syms M4
g = gamma4;
eqn = (A4/A5)^((2*g-2)/(g+1)) == ((M4^(4/(g+1)))*(g-1)/(g+1)) + (M4^((2-(2*g))/(g+1)))*2/(g+1);
S = vpasolve(eqn,M4,[0 1]);
M4 = double(S);
%Continuing the location 4 calculations
Pt4 = Pt3*Pt4_Pt3;
P4 = Pt4/(1+(gamma4-1)/2*M4^2)^(gamma4/(gamma4-1));
T4 = Tt4/(1+(gamma4-1)/2*M4^2);
```

```
a4 = sqrt(gamma4*R*T4);
V4 = a4*M4;
rho4 = P4/(R*T4);

%Results and figures
Fs = T/m_a                %Specific Thrust (m/s)
Is = T/(m_f*9.81)         %Fuel Specific Impulse (s)
TSFC = m_f/T*10^6         %Thrust Specific Fuel Consumption (g/kN*s)
prop_eff = (T*V0) / ( (m_t*(V6^2)/2) - (m_a*(V0^2)/2) )
ther_eff = ( (m_t*(V6^2)/2) - (m_a*(V0^2)/2) ) / (m_f*Qr*b_eff)
overall_eff = prop_eff*ther_eff

% x=1 location data is added by looking at the other code
% This is the location where nomal shock occured
M1 = 0.7252;
P1 = 302310;
T1 = 555.9853;
Pt1 = Pt0*Pt1_Pt0;
Tt1 = Tt0/(Tt0_Tt1);
V1 = 342.7723;
rho1 = 1.8943;
A1 = 0.0563;

%enthalpy at each location
h0 = Cp1*T0;
ht1 = Cp1*Tt1;
ht2 = Cp1*Tt2;
ht3 = Cp1*Tt3;
ht4 = Cp4*Tt4;
ht5 = Cp4*Tt5;
h6 = Cp4*T6;

%entropy at each point
s0 = (Cp1*log(T0)) - (R*log(P0));
st1 = (Cp1*log(Tt1)) - (R*log(Pt1));
st2 = (Cp1*log(Tt2)) - (R*log(Pt2));
st3 = (Cp1*log(Tt3)) - (R*log(Pt3));
st4 = (Cp4*log(Tt4)) - (R*log(Pt4));
st5 = (Cp4*log(Tt5)) - (R*log(Pt5));
s6 = (Cp4*log(T6)) - (R*log(P6));

x = [0 1 2 3 4 5 6];        %location of each stage
M = [M0 M1 M2 M3 M4 M5 M6];
P = [P0 P1 P2 P3 P4 P5 P6];
T = [T0 T1 T2 T3 T4 T5 T6];
Pt = [Pt0 Pt1 Pt2 Pt3 Pt4 Pt5 Pt6];
Tt = [Tt0 Tt1 Tt2 Tt3 Tt4 Tt5 Tt6];
Ttv2 = [T0 Tt1 Tt2 Tt3 Tt4 Tt5 T6];
ht = [h0 ht1 ht2 ht3 ht4 ht5 h6];
st = [s0 st1 st2 st3 st4 st5 s6];

figure (1)
plot(x,M);
title('Mach Number distribution', 'FontSize', 11)
grid on
```

```
hold on
xlabel('x', 'FontSize', 12)
ylabel('Mach', 'FontSize', 12)

figure (2)
plot(x,P);
title('Pressure distribution', 'FontSize', 11)
grid on
hold on
xlabel('x', 'FontSize', 12)
ylabel('Pressure', 'FontSize', 12)

figure (3)
plot(x,Pt);
title('Total Pressure distribution', 'FontSize', 11)
grid on
hold on
xlabel('x', 'FontSize', 12)
ylabel('Total pressure', 'FontSize', 12)

figure (4)
plot(x,Tt);
title('Total Temperature distribution', 'FontSize', 11)
grid on
hold on
xlabel('x', 'FontSize', 12)
ylabel('Total temperature', 'FontSize', 12)

figure (5)
plot(x,T);
title('Temperature distribution', 'FontSize', 11)
grid on
hold on
xlabel('x', 'FontSize', 12)
ylabel('Temperature', 'FontSize', 12)

figure (6)
plot(st,Ttv2);
title('T-s graph', 'FontSize', 11)
grid on
hold on
xlabel('Entropy', 'FontSize', 12)
ylabel('Temperature', 'FontSize', 12)

figure (7)
plot(st,ht);
title('h-s graph', 'FontSize', 11)
grid on
hold on
xlabel('Entropy', 'FontSize', 12)
ylabel('Enthalpy', 'FontSize', 12)
```

A.2. Engine Inlet

```
clear
clc

M0 = 3.03;
gamma = 1.4;          %gamma of air
P0 = 13500;           %P at 14275 m
T0 = 216.65;          %T at 14275 m
R = 287.05;
rho0 = P0/(R*T0);     %air density
m_a = 36.5296;        %mass flow rate
Pt0 = P0*(1+(gamma-1)/2*M0^2)^(gamma/(gamma-1));

%First oblique shock
beta1 = 27.1*(pi/180);              %Wave angle as input
theta1 = atan(2/tan(beta1)*(M0^2*sin(beta1)^2-1)/(M0^2*(gamma+cos(2*beta1))+2));
theta1deg = theta1*180/pi;        %Turn angle
Mn0 = M0*sin(beta1);
Mn1_1 = sqrt((1+(gamma-1)/2*Mn0^2)/(gamma*Mn0^2-(gamma-1)/2));
M1_1 = Mn1_1/sin(beta1-theta1);   %Mach number after the oblique shock

P1_1 = P0*((2*gamma*M0^2*(sin(beta1))^2-(gamma-1))/(gamma+1));
rho1_1 = rho0*((M0^2*(sin(beta1))^2*(gamma+1))/(M0^2*(sin(beta1))^2*(gamma-1)+2));
T1_1 = T0*(P1_1*rho0)/(P0*rho1_1);
Pt1_1 = P1_1*(1+(gamma-1)/2*M1_1^2)^(gamma/(gamma-1));
PR1 = Pt1_1/Pt0;

%Second oblique shock
beta2 = 34.4*(pi/180);
theta2 = atan(2/tan(beta2)*(M1_1^2*sin(beta2)^2-1)/(M1_1^2*(gamma+cos(2*beta2))+2));
theta2deg = theta2*180/pi;
Mn2_2 = M1_1*sin(beta2);
Mn1_2 = sqrt((1+(gamma-1)/2*Mn2_2^2)/(gamma*Mn2_2^2-(gamma-1)/2));
M1_2 = Mn1_2/sin(beta2-theta2);

P1_2 = P1_1*((2*gamma*M1_1^2*(sin(beta2))^2-(gamma-1))/(gamma+1));
rho1_2 = rho1_1*((M1_1^2*(sin(beta2))^2*(gamma+1))/(M1_1^2*(sin(beta2))^2*(gamma-1)+2));
T1_2 = T1_1*(P1_2*rho1_1)/(P1_1*rho1_2);
Pt1_2 = P1_2*(1+(gamma-1)/2*M1_2^2)^(gamma/(gamma-1));
PR2 = Pt1_2/Pt1_1;

%Third oblique shock
beta3 = 45.6*(pi/180);
theta3 = atan(2/tan(beta3)*(M1_2^2*sin(beta3)^2-1)/(M1_2^2*(gamma+cos(2*beta3))+2));
theta3deg = theta3*180/pi;
Mn3_3 = M1_2*sin(beta3);
Mn1_3 = sqrt((1+(gamma-1)/2*Mn3_3^2)/(gamma*Mn3_3^2-(gamma-1)/2));
M1_3 = Mn1_3/sin(beta3-theta3);

P1_3 = P1_2*((2*gamma*M1_2^2*(sin(beta3))^2-(gamma-1))/(gamma+1));
rho1_3 = rho1_2*((M1_2^2*(sin(beta3))^2*(gamma+1))/(M1_2^2*(sin(beta3))^2*(gamma-1)+2));
T1_3 = T1_2*(P1_3*rho1_2)/(P1_2*rho1_3);
Pt1_3 = P1_3*(1+(gamma-1)/2*M1_3^2)^(gamma/(gamma-1));
PR3 = Pt1_3/Pt1_2;
```

```
%Normal shock
beta4 = 90*(pi/180);
theta4 = atan(2/tan(beta4)*(M1_3^2*sin(beta4)^2-1)/(M1_3^2*(gamma+cos(2*beta4))+2));
theta4deg = theta4*180/pi;
Mn4_4 = M1_3*sin(beta4);
Mn1_4 = sqrt((1+(gamma-1)/2*Mn4_4^2)/(gamma*Mn4_4^2-(gamma-1)/2));
M1_4 = Mn1_4/sin(beta4-theta4);

P1_4 = P1_3*((2*gamma*M1_3^2*(sin(beta4))^2-(gamma-1))/(gamma+1));
rho1_4 = rho1_3*((M1_3^2*(sin(beta4))^2*(gamma+1))/(M1_3^2*(sin(beta4))^2*(gamma-1)+2));
T1_4 = T1_3*(P1_4*rho1_3)/(P1_3*rho1_4);
Pt1_4 = P1_4*(1+(gamma-1)/2*M1_4^2)^(gamma/(gamma-1));
PR4 = Pt1_4/Pt1_3;

%area calculation for throat (A1_4)
a1_4 = sqrt(gamma*R*T1_4);
V1_4 = a1_4*M1_4;
A1_4 = m_a/(rho1_4*V1_4);

%result
PRt = PR1*PR2*PR3*PR4;
```

B) CAD Design

B.1. CAD Drawing for the ConDi Nozzle

Figure 32. The view of the ConDi nozzle.[SolidWorks]

The figure 32 shows the view of the ConDi nozzle. This part of the engine has been drawn by using SolidWorks.

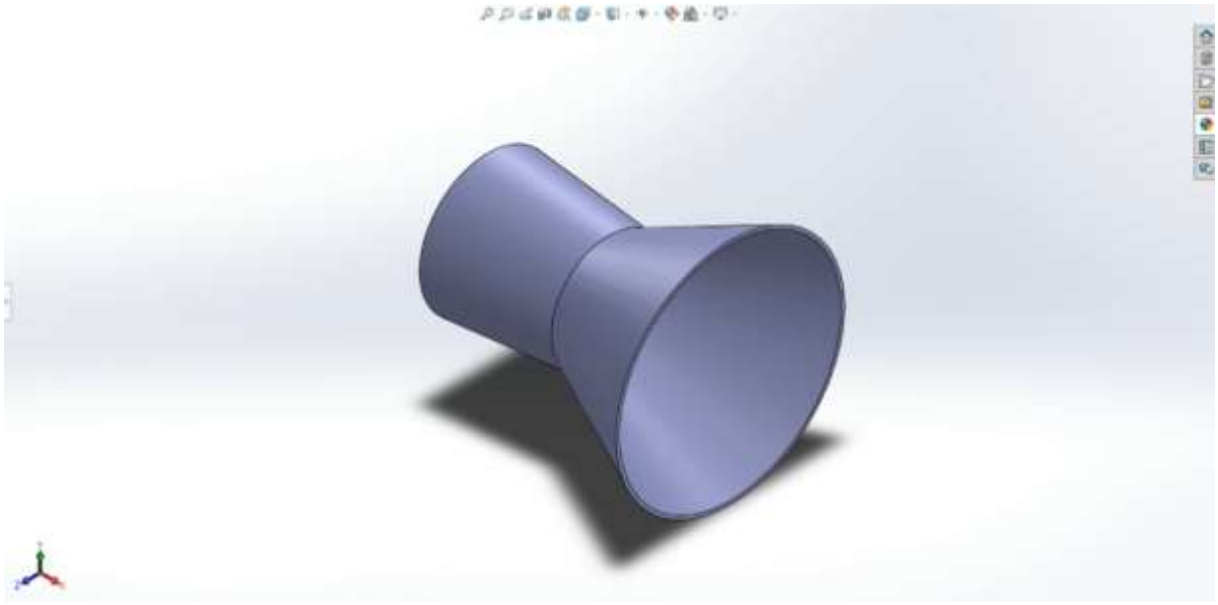

Figure 33. The view of the ConDi nozzle.[SolidWorks]

The figure 33 exhibits the view of the ConDi nozzle. This part of the engine has been drawn by using SolidWorks.